Appendix D: Late Cretaceous (Maastrichtian) shallow water hydrocarbon seeps from Snow Hill and Seymour Islands, James Ross Basin, Antarctica

Crispin T.S. Little[a*], Daniel Birgel[b], Adrian J. Boyce[c], J. Alistair Crame[d], Jane E. Francis[d], Steffen Kiel[e], Jörn Peckmann[b], Duncan Pirrie[f], Gavyn K. Rollinson[g] and James D. Witts[a]

[a]School of Earth and Environment, University of Leeds, Leeds LS2 9JT, UK

[b]Department of Geodynamics and Sedimentology, Center for Earth Sciences, University of Vienna, 1090 Vienna, Austria

[c]SUERC, Rankine Avenue, Scottish Enterprise Technology Park, East Kilbride, G75 0QF, UK

[d]British Antarctic Survey, High Cross, Madingley Road, Cambridge CB3 0ET, UK

[e]Geoscience Center, Georg-August University of Göttingen, Geobiology Group, Goldschmidtstrasse 3, 37077 Göttingen, Germany

[f]Helford Geoscience LLP, Menallack Farm, Trelowarren Mill Barn, Mawgan, Helston, Cornwall, TR2 6AE, UK

[g]Camborne School of Mines, CEMPS, University of Exeter, Penryn Campus, Cornwall TR10 9FE, UK

*Corresponding author; telephone/fax number: +44 (0)113 3436621/+44 (0)113 343 5259; email address: earctsl@leeds.ac.uk.

D1: Abstract

Fossil hydrocarbon seeps are present in latest Cretaceous (Maastrichtian) volcaniclastic shallow shelf sediments exposed on Snow Hill and Seymour Islands, James Ross Basin, Antarctica. The seeps occur in the Snow Hill Island Formation on Snow Hill Island and are manifest as large-sized, cement-rich carbonate bodies, containing abundant thyasirid bivalves and rarer ammonites and solemyid bivalves. These bodies have typical seep cement phases, with $\delta^{13}C$ values between −20.4 and −10.7‰ and contain molecular fossils indicative of terrigenous organic material and the micro-organisms involved in the anaerobic oxidation of methane, including methanotrophic archaea and sulphate-reducing bacteria. On Seymour Island the seeps occur as micrite-cemented burrow systems in the López de Bertodano Formation and are associated with thyasirid, solemyid and lucinid bivalves, and background molluscan taxa. The cemented burrows also have typical seep cement phases, with $\delta^{13}C$ values between −58.0 and −24.6‰. There is evidence from other data that hydrocarbon seepage was a common feature in the James Ross Basin throughout the Maastrichtian and into the Eocene. The Snow Hill and Seymour Island examples comprise the third known area of Maastrichtian hydrocarbon seepage. But compared to most other ancient and modern seep communities, the James Ross Basin seep fauna is of very low diversity, being dominated by infaunal bivalves, all of which probably had thiotrophic chemosymbionts, but which were unlikely to have been seep obligates. Absent from the James Ross Basin seep fauna are ‘typical’ obligate seep taxa from the Cretaceous and the Cenozoic. Reasons for this may have been temporal, palaeolatitudinal, palaeobathymetric, or palaeoecological.

Keywords: Hydrocarbon seeps; palaeoecology; chemosynthetic ecosystems; bivalves; Cretaceous

D2: Introduction

Hydrocarbon seeps are shallow to deep water (as much as 7 km water depth) sites around the continental margins, in both active and passive settings, where hydrocarbon-rich fluids leak onto the seafloor, forming structures such as pockmarks and mud volcanoes (e.g. Judd and Hovland, 2009, and references therein). Much of the seeping hydrocarbons comprises methane, both of thermogenic and biogenic origin, deriving from underlying thick, organic-rich sedimentary sequences. In the shallow subsurface at seep sites methane is utilized by a consortium of methanotrophic archaea and sulphate-reducing bacteria (SRB) in the anaerobic oxidation of methane (AOM) reaction (e.g. Hinrichs et al., 1999; Boetius et al,. 2000; Reitner et al,. 2005), leading to the supersaturation of pore fluids with respect to carbonate ions and resulting in the formation of distinctive carbonate deposits with multi-phase carbonate cements and very negative $\delta^{13}C$ values (e.g. Ritger et al., 1987; Aloisi et al., 2000; Naehr et al., 2007; Haas et al., 2010). Molecular fossils (biomarkers) of the AOM reaction, also with characteristic negative $\delta^{13}C$ values, are commonly preserved in modern and ancient seep carbonates (e.g. Peckmann et al., 1999; Thiel et al., 1999; Elvert et al., 2000; Bouloubassi et al., 2006; Birgel et al., 2008b). Hydrocarbon seeps support diverse and high-biomass communities of macrofauna, which are dominated by taxa having symbiotic relationships with chemotrophic bacteria (principally methanotrophs and thiotrophs). These taxa include bivalves (e.g. solemyid, vesicomyid, lucinid and thyasirid clams, and bathymodiolin mussels) and siboglinid (vestimentiferan) tubeworms (e.g. Paull et al., 1984; Sibuet and Olu, 1998; Levin, 2005; Dubilier et al., 2008). Representatives of the solemyids, lucinids and thyasirids are also common in other environments where reducing sediments predominate (Oliver and Killeen, 2002; Taylor and Glover, 2006; Taylor et al., 2008). There is evidence for a bathymetric control on the ecological and taxonomic structure of modern hydrocarbon seep communities. The number of taxa restricted to seep sites (i.e. obligate taxa) decreases from the slope and deep shelf onto the shallow shelves, such that most obligate chemosymbiotic taxa (such as the vesicomyid clams and bathymodiolin mussels) disappear above around 200 m. In contrast, the number of predators and background taxa increases from slope to shallow shelf (Levin et al., 2000; Sahling et al., 2003; Cordes et al., 2007; Dando, 2010). Bathymetric controls

are also evident on seep faunas in the Cenozoic and the late Mesozoic (Amano et al., 2010; Kiel, 2010a).

The fossil record of seep communities is becoming increasingly well known (e.g. Campbell, 2006), especially for the Mesozoic and Cenozoic, and some important macroevolutionary trends are emerging. The Mesozoic fossil seep assemblages contain a variety of dominant obligate ('endemic') taxa, including the dimerelloid brachiopods, the gastropod genus *Paskentana*, and family Hokkaidoconchidae, and the bivalve genus *Caspiconcha*, none of which are found in Cenozoic seep communities (Kiel and Little, 2006; Kiel, 2010b, and references therein). Instead, from the Eocene onwards, fossil seep communities contain ubiquitous examples of vesicomyids and bathymodiolins, and are structured ecologically much like modern seep communities (Goedert and Squires, 1990; Kiel, 2010b). The time period between the latest Mesozoic and the earliest Cenozoic is therefore of interest in elucidating this evolutionary transition, and yet there are very few recorded seep sites of this age: the youngest Tepee Buttes seep deposits of the Western Interior Basin of the USA are Early Maastrichtian (69.1 Ma and older) in age (Metz, 2010), the Sada Limestone seep in Japan is dated as Campanian-Maastrichtian (Nobuhara et al., 2008), and there is one example of a Paleocene seep from California (Schwartz et al., 2003; Kiel, 2013). Further, the macroevolutionary trends in fossil seep faunas so far identified are based largely on data from seeps in the lower latitudes of the Northern Hemisphere; information from the high latitudes in the Southern Hemisphere is particularly sparse, with examples from Late Jurassic of Alexander Island, Antarctica (Kaim and Kelly, 2009) and from the mid- to late Cretaceous of New Zealand (Kiel et al., 2013). This situation is mirrored by the record of modern seeps from Southern high latitudes, which comes from off Chile (e.g. Sellanes et al., 2004),the Hikurangi margin of New Zealand (Baco et al., 2010), and, in Antarctica, the finding in 2005 of clusters of dead vesicomyid shells in 850 m water depth in the Weddell Sea after the collapse of the Larsen B Ice Shelf (Domack et al., 2005; Niemann et al., 2009).

Here we report an integrated petrological, geochemical (stable isotopes and biomarkers) and palaeontological study of hydrocarbon seeps from latest Cretaceous (Maastrichtian) volcaniclastic shallow shelf sediments exposed on

Snow Hill and Seymour Islands, James Ross Basin, Antarctica. The seeps are manifest as large-sized, cement-rich carbonate bodies on Snow Hill Island and micrite-cemented burrow systems on Seymour Island. They are associated with low diversity faunas of thyasirid, solemyid and lucinid bivalves, which we discuss in light of existing ideas about the macroevolutionary history of seep communities.

D3: Geological setting

D3.1: Lithostratigraphy and palaeoenvironments

The James Ross Basin is a large extensional sedimentary basin that formed behind the magmatic arc of the Antarctic Peninsula from the late Mesozoic to early Cenozoic (e.g. Pirrie et al., 1997; Crame et al., 2004; Olivero, 2012). The volcaniclastic sediments deposited in this basin are now exposed on the various islands in the James Ross Island area, including Snow Hill and Seymour Islands (subsequently SHI and SI respectively; Fig. 1). On many of the islands the outcrop extent is exceptional (up to 100% on SI), because there is no significant vegetation at this latitude. The Late Cretaceous infill of the James Ross Basin is particularly thick, comprising approximately 2150 m of Campanian and Maastrichtian fine grained sediments, and forms part of the Coniacian to Danian aged Marambio Group (Pirrie et al., 1997; McArthur et al., 2000; Crame et al., 2004; Olivero, 2012). The Maastrichtian part of the group makes up most of the Snow Hill Island Formation (SHIF) and overlying López de Bertodano Formation (LBF) (Fig. 2). The top two units of the SHIF on SHI are the Karlsen Cliffs Member (KCM) below and the Haslum Crag Member (HCM) above (Fig. 2; Zinsmeister, 1998). These two units crop out on the Spath Peninsula at the northern tip of SHI, and along strike on the south western tip of SI (Fig. 1). The KCM consists of mudstones, sandy mudstones and heavily bioturbated fine sandstones with abundant early diagenetic concretions (Pirrie et al., 1997), interpreted by Olivero (2012) to represent sediments formed in a coarsening upwards prograding deltaic wedge. The HCM of Pirrie et al. (1997) is roughly equivalent to the Haslum Crag Sandstone of Olivero (2012) and comprises medium- to coarse-grained cross-

stratified and channelized sandstones, passing upwards into intensely bioturbated finer grained sandstones and siltstones, containing fossiliferous concretions (Pirrie et al., 1997). The HCM is separated from the KCM by an unconformity, represented by a thin, framework-supported conglomerate of reworked clasts (Pirrie et al., 1997; Crame et al., 2004). Olivero (2012) interprets the Haslum Crag Sandstone as being forced regressive tidal deposits (Olivero, 2012; fig. 2). The LBF crops out on the eastern side of the Spath Peninsula of SHI (lower part only) and extensively on the western side of SI (full thickness; Fig. 1). The LBF contains the Cretaceous-Paleogene (K–Pg) boundary near its top (Fig. 2; Crame et al., 2004; Olivero, 2012; Tobin et al., 2012). Lithologically the LBF is dominated by intensely bioturbated muddy siltstones, with thin intercalated sandstones and discontinuous concretionary levels, one of which, at locality D5.345.2, was the site of extensive study reported in this paper. The LBF coarsens upwards slightly towards the top of the section where there are some prominent glauconitic sandstones (Crame et al., 2004). According to Olivero (2012) the lower part of the LBF comprises estuarine and shallow marine deposits, the middle part transgressive shelf deposits, and the top part regressive shelf deposits (Olivero, 2012; fig. 2). Palaeotemperature estimates derived from oxygen isotope analysis of molluscan shell material within the LBF indicate mean annual seawater temperatures on the Antarctic shelf ranged from ~5 to - 8°C at this time (Pirrie and Marshall, 1990; Dutton et al., 2007; Tobin et al., 2012), consistent with an overall cooling trend seen globally during the Maastrichtian (e.g. Friedrich et al., 2012).

D3.2: Biostratigraphy and chronostratigraphy

Precise dating of the James Ross Basin sediments to lower latitude sections is hampered by a number of issues which make correlation to well-dated Late Cretaceous IODP/DSDP ocean drill-cores and stratigraphic sections in the northern hemisphere problematic. Both macro and microfossil faunas and floras show a high degree of endemism (e.g. Macellari, 1986; Zinsmeister and Macellari, 1988; Pirrie et al., 1997; Olivero and Medina, 2000; Crame et al., 2004; Bowman et al., 2012; Olivero, 2012), and several key groups useful for

biostratigraphy elsewhere such as certain ammonites and inoceramid bivalves, either disappear from the Antarctic record during the Campanian (Zinsmeister and Feldmann, 1996; Crame et al., 1996; Crame and Luther, 1997; McArthur et al., 2000; Olivero and Medina, 2000; Olivero, 2012) or are absent from the James Ross Basin record entirely. Dinoflagellate cysts may provide the best opportunity for microfossil biostratigraphy of the basin due to the paucity of other groups such as foraminifera (Pirrie et al, 1997; Bowman et al., 2012; 2013), but correlation to lower latitudes is still problematic and key stratigraphic sections such as those on SHI await revision.

In terms of macrofossils, ammonites appear to hold the most promise for biostratigraphic zonation and comparison with other sections. They are among the most common fossils found throughout the Late Cretaceous sequence (Macellari, 1986; Olivero, 1984; 1988; 1992; 2012; Crame et al., 2004; Kennedy et al., 2007) and provide an important stratigraphic reference for correlating sections across the entire basin (Pirrie et al, 1997; Olivero and Medina, 2000; Crame et al., 2004; Olivero et al., 2008; Olivero, 2012). Olivero and Medina (2000) and Olivero (2012) divide the James Ross Basin into 14 distinct ammonite assemblages, based mainly on the stratigraphic distribution of the family Kossmaticeratidae, which contains many endemic taxa. The KCM and HCM occur in assemblage 10, which is also present in the Cape Lamb Member of the SHIF on Vega Island. Detailed stratigraphic range data for ammonite taxa from the KCM and HCM have never been illustrated, but the fauna appears to be dominated by specimens belonging to the kossmaticeratid genera *Gunnarites*, most probably the highly variable *Gunnarites antarcticus*. Other ammonites reported from the KCM and HCM are indicative of a Late Campanian to Maastrichtian age when compared with lower latitude sections, such as those in South America, South Africa, Australia and New Zealand (Charrier and Lahsen, 1968; Henderson, 1970; Kennedy and Klinger, 1985; Henderson and McNamara, 1985; Walaszczyk et al., 2009; Salazar et al., 2010; Stinnesbeck et al., 2012). They also form a distinctly different assemblage to those found stratigraphically higher in the LBF on SI (see below and Crame et al., (2004)). This biostratigraphic interpretation is consistent with strontium isotope data from the age-equivalent

Cape Lamb Member on Vega Island (Crame et al., 1999; McArthur et al., 2000), which suggests an early Maastrichtian age for this unit.

Biostratigraphic zonation of the LBF on SI using ammonites is similarly hampered by the dominance of endemic kossmaticeratid taxa. The studied concretion-rich layer at locality D5.345.2 is located in ammonite assemblage 11 of Olivero and Medina (2000) and Olivero (2012). A single well-preserved specimen of *Maorites seymourianus* was found at this locality (Fig. 5D), whilst nearby equivalent horizons have also yielded specimens of *Maorites* (probably *seymourianus*) and *Kitchinites darwini* (see also Macellari, 1986). Other reported taxa from this stratigraphic interval include *Diplomoceras cylindraceum*, *Pseudophyllites loryi* and *Neophylloceras* sp. (Olivero, 2012). All of these taxa are consistent with a Maastrichtian age for these deposits. Strontium isotope data (McArthur et al., 1998; Crame et al., 2004), and recent biostratigraphic studies using marine palynology (Bowman et al., 2012; 2013), suggest all of the HCM and LBF exposed on SI below the K–Pg boundary are early to latest Maastrichtian in age when compared to other Southern Hemisphere sections. A recent magnetostratigraphic study of the LBF (Tobin et al., 2012) identified several magnetic polarity reversals which can be correlated with both lower latitude sections and a recently revised global Maastrichtian timescale (e.g. Husson et al., 2011; Gardin et al., 2012; Voigt et al., 2012), as well as new age models for the SI succession (Bowman et al., 2013). This work suggests the Cretaceous portion of the LBF on SI spans magnetochrons C31R through to C29R and was therefore deposited between ~70 and 66 Ma – the currently accepted date of the K–Pg boundary (Husson et al., 2011; Voigt et al., 2012; Tobin et al., 2012). Based on application of the data presented in Tobin et al. (2012) to measured sections used herein (see also Bowman et al. 2013) the concretion-rich layer at locality D5.345.2 occurs somewhere in the upper part of chron C31R, indicating a date of ~69 Ma (Husson et al., 2011; Voigt et al., 2012; Fig. 2).

D4: Materials and methods

Rock samples and fossils were collected from SHI and SI during a series of field seasons to the James Ross Basin area by the British Antarctic Survey (BAS) and collaborators from ~1994 to 2007 and are stored in the BAS collections and those in the School of Earth and Environment, University of Leeds. A subset of these samples from the carbonate-cemented layers and associated fossils on SHI and the concretion-rich layer at locality D5.345.2 on SI were selected for additional analysis (Table 1). Additional samples from SI come from the Zinsmeister collection housed in the Paleontological Research Institution, Ithaca, New York, USA (Table 1).

D4.1: Petrography

Three samples from SHI were analysed petrographically at Helford Geoscience LLP (Table 1). Multiple uncovered polished thin sections were prepared from the samples. Each thin section was scanned and examined under polarised light microscopy, using cathodoluminescence (CL) and following carbonate staining. The mineralogy and texture of three representative thin sections was quantified using automated SEM-EDS analysis using QEMSCAN® technology (see Pirrie et al., 2004, 2014). The sections were carbon coated and then the whole area of each thin section was scanned using a 10 μm beam stepping interval; subsequently smaller areas of the thin section were also measured using a 5 μm beam stepping interval. Five samples from SI were analysed petrographically using covered and uncovered thin sections under light microscopy at the University of Leeds and Georg-August Universität Göttingen (Table 1), and one of these was micro-drilled for X-ray diffraction (XRD) analysis at the University of Leeds using a Bruker D8 with a Cu K alpha source and configured to a vertical theta/2 theta Bragg-Brentano reflection stage, and with a Lynxeye detector. Phase identification was achieved using Bruker's EVA software with the ICDD PDF2 database.

D4.2: Carbonate stable carbon and oxygen isotopes

Samples from the petrographic specimens and others from SHI and SI were micro-drilled to produce powders, and were analysed at the Scottish Universities Environmental Research Centre, East Kilbride and the Georg-August Universität Göttingen. At East Kilbride CO_2 was quantitatively released from the powered samples by standard *in vacuo* digestion with 100% phosphoric acid at 25°C. Gases thus produced were analysed on a VG SIRA 10 mass spectrometer, monitoring mass to charge ratios of 44, 45 and 46. Analytical raw data were corrected using standard procedures (Craig, 1957). The error of reproducibility, based on complete analysis of internal standards (including acid digestion) was ±0.1‰ for $\delta^{13}C$ values, and ±0.2‰ for $\delta^{18}O$ values. At Göttingen, the powered samples were reacted with 100% phosphoric acid at 75°C using a Finnigan Kiel IV Carbonate Device attached to a Finnigan DELTA V PLUS mass spectrometer. Reproducibility was checked by replicate analysis of laboratory standards and was better than ±0.05‰. All isotope data are given as δ values in per mil (‰) relative to the Vienna Peedee belemnite (V-PDB) standard.

D4.3: Lipid biomarkers

A single sample (Sn1-1) from SHI, previously drilled for isotope analysis, was analysed for biomarkers at the Centre of Marine Environmental Sciences (MARUM), Bremen University (Table 1). The preparation and decalcification procedure was performed after a method described in Birgel et al. (2006b). After the saponification procedure with KOH (6%) in methanol, the sample was extracted with a microwave extraction system (CEM MARS X) at 80°C and 300 W with a 3:1 dichloromethane-methanol mixture. The separation of the total lipid extract was performed after Birgel et al. (2008a). The resulting hydrocarbons and carboxylic acids fractions were measured with a Thermo Electron Trace MS gas chromatograph-mass spectrometer, equipped with a 30 m *Rxi*-5 MS fused silica column (0.25 mm inside diameter, 0.25 µm film thickness), using helium as the carrier gas. The temperature program was: 60°C, 1 min isothermal; from 60 to 150°C at 10°C/min, from 150 to 320°C at

4°C/min; 22 min isothermal at 320°C. Identification of individual compounds was based on retention times and published mass spectra. Compound-specific carbon isotope analysis of the molecular fossils was performed with a Thermo Electron Trace GC Ultra connected via a Finnigan combustion interface-II to a Finnigan MAT 252 mass spectrometer. Conditions of the gas chromatograph were identical to those described above. Carbon isotopes are given as δ values in per mil (‰) relative to the Vienna Peedee belemnite (V-PDB) standard. Each measurement was calibrated using several pulses of CO_2 with known isotopic composition at the beginning and end of the run. Instrument precision was checked with a mixture of *n*-alkanes (C_{15} to C_{29}) of known isotopic composition. The analytical standard deviation was < 0.8‰.

D5: Results

D5.1: Carbonate bodies and 'Thyasira' occurrences on Snow Hill Island

Specimens of the large thyasirid bivalve '*Thyasira' townsendi* are common in the lower part of the type section of the KCM on the Spath Peninsula at Thyasira Hill (64.3748ºS, 56.9807ºW; Fig. 1). Here the first '*T.' townsendi* are found at the 30 m mark in BAS section DJ.616 of Pirrie et al. (1997) occurring initially as articulated singletons, both *in situ* (i.e. with the plane of the dorsal commissure vertical) and displaced to lie on one valve or the other. Numbers of specimens increases very rapidly up section to reach, in places, an estimated density of >120/m^2 (Fig. 3C). Between approximately 30 and 65 m in section DJ.616 clusters of '*T.' townsendi* are increasingly associated with patches of pale blue-grey carbonate cementation which serve to accentuate the regular, planar bedding (Fig. 3B,D). Initially the cemented regions are 20 to 30 cm thick and 50 to 100 cm in width but at higher levels the beds are more continuous and weather out to form the peak of a prominent structure 60 m in height that forms the summit of Thyasira Hill (Figs. 3A, 4A,C). This feature is located approximately 500 m SW of Nordenskjöld's Hut. At Thyasira Hill the carbonate cemented beds are 30 to 75 cm thick and sheet-like on the scale of exposure. The internal texture of the best cemented beds is very

much that of a shell bed that in places verges into a coquina (Figs. 3E, 4C). Many of the '*T.' townsendi* shells (Fig. 5G) are in growth position, but it is noticeable that they rarely touch each other (Fig. 4C, 5A); others are clearly *ex-situ* and some of these are broken. A number of small ammonites, and ammonite fragments, are also preserved in the cemented layers (Fig. 3E). These are mostly referable to *Gunnarites* (Fig. 5E) and occasional *Anagaudryceras* and many appear to be juveniles. Their disposition is such as to suggest that they could have been current-swept into the '*Thyasira'* layers. The interbeds between the well-cemented layers have yielded isolated articulated specimens of '*T.' townsendi* together with small ammonites, including *Jacobites anderssoni* (Fig. 5F), and possible *Gunnarites bhavaniformis* (Fig. 5E), and scattered tube specimens of the serpulid worm *Austrorotularia* sp. About 200 m across a small valley to the South of Thyasira Hill at the same stratigraphic level are approximately 12 topographic knolls up to 10 m tall and ~5 m wide (Fig. 3B,D), which represent carbonate cemented patches that have been exhumed by weathering from the enclosing fine-grained sediments of the KCM. These knolls have similar lithologies and faunal content to Thyasira Hill, including the ammonite *Gunnarites antarcticus,* the solemyid bivalve *Solemya rossiana* and an indeterminate high-spired gastropod. Carbonate cemented '*Thyasira'* layers and patches continue between 65 and 80 m in the section DJ.616, but are not observed in the topmost 20 to 25 m. It should be emphasized that the well-cemented '*Thyasira'* patches and layers are markedly discontinuous both laterally and vertically. They occur through an approximately 50 m thick section of DJ.616 (i.e. ~30 and 80 m), but at no other stratigraphic level within the KCM. Equally, they cannot be traced laterally in the extensive headwall of the small valley system immediately to the SW of Nordenskjöld's Hut. The cementation is patchy and discontinuous over perhaps a 100 m distance horizontally and a 50 m stratigraphical thickness.

D5.2: Carbonate concretions and 'Thyasira' occurrences on Seymour Island

'*Thyasira' townsendi* occurs intermittently in laterally discontinuous layers, usually within a distinctive dark sulphurous mudstone facies, throughout the rest of the nearly 1500 m thick Maastrichtian succession on SHI and SI. In these layers '*T.' townsendi* often occurs together with articulated specimens of the lucinid bivalve '*Lucina' scotti* (Fig. 5J) and/or the solemyid bivalve *Solemya rossiana*. However, unlike in the KCM, the stratigraphically later '*T.' townsendi* layers in the HCM and LBF are not associated with well-cemented large carbonate deposits. The '*T.' townsendi* layers occur in several places in the LBF on SI (Table 1). One of these, at locality D5.345.2, 458 m above the basal unconformity with the HCM (Fig. 2), contains scattered carbonate-cemented concretions together with abundant specimens '*T.' townsendi* (Fig. 5H) and *S. rossiana* (Fig. 5K) and some examples of the ammonite *Moarites seymourianus* (Fig. 5D). There are also large numbers of the nuculid bivalve *Leionucula suboblonga,* small examples of the trigoniid *Oistrigonia pygoscelium* and the gastropod *"Cassidaria" mirabilis.* Horizons immediately adjacent to D5.345.2 also yield examples of the bivalves *Nordenskjoldia nordenskjoldi, Cucullaea antarctica,* and a small indeterminate veneroid. These molluscan taxa are a good representation of the 'background' benthic molluscan fauna found throughout this portion of the LBF on SI (e.g. Crame et al., 2004). The last occurrence of the distinctive '*T.' townsendi* facies occurs in section line DJ.953, 48 m below the K–Pg boundary in the LBF (Figs. 1 and 2). However, a single specimen of '*T.' townsendi* was recently collected from the 237-250 m level in the Paleocene Sobral Formation, i.e. ~300 m above the K–Pg boundary.

The concretions at locality D5.345.2 are fairly diverse in size and shape. Some have a roughly cyclindrical shape, are between 11 and 18 mm in diameter and up to 39 mm in length (Fig. 5B). These are largely composed of dark grey fine-grained sediments cemented by micrite with a later, weathering rind of gypsum, but some also have internal infillings of fibrous calcite cements (Fig. 6B). Other concretions are roughly circular, between 31 and 49 mm in diameter and have pale-coloured *Planolites*-like burrows on their surfaces

(Fig. 5B). Internally these concretions are formed of dark grey fine-grained sediments, within which similar burrows can often be seen.

D5.3: Petrography

The samples (DJ.731.14 and DJ.633.3) from carbonate cemented bodies in the KCM on SHI comprise muddy to silty very fine grained sandstones composed of angular grains of detrital quartz, plagioclase and microcline, along with abundant biotite and diagenetic glauconite, minor muscovite, and occasional framboidal pyrite and wood fragments, including examples of *Cupressinoxylon* or *Podocarpoxylon* (Figs. 6A,C,D; 7C). Texturally the sediments have a bioturbated fabric; locally with a peloidal texture with oval faecal pellets. The sediments are tightly cemented by a non-ferroan micritic to microsparry calcite (Figs. 6A,C,D; 7C), and this commonly causes splaying of biotite micas with the growth of calcite cements parallel to the mineral cleavage. This cement phase we label m1 is thought to correspond to similar phases in Kiel et al. (2013). The micrite and microspar are intergrown with and post-dated by two main generations of ferroan calcite cement, which are bright orange luminescent under CL (Fig. 7C). Cross-cutting the sediments are pipe-like structures (which we interpret as fluid conduits in section 5) up to several centimetres in length, filled by numerous generations of carbonate cements (Figs. 6A,C,D; 7A-C). These cements are nucleated onto the surrounding sandstones and also overgrow faecal pellets. The cement infills within these pipe-like structures are complex, with up to six zones per pipe of a non-ferroan, fibrous calcite cement with banded and botryoidal textures (termed bbc; Fig. 7A,B). Under CL this fibrous cement shows complex zones of alternating bright and less bright orange luminescence (Fig. 7C). QEMSCAN® mapping shows that within some of the pipe fills there is a zone of carbonate cement containing Fe and Mn (probably ankerite) which post-dates, and is in turn post-dated by, fibrous calcite cements (Figs. 6C-D; 7B). In addition, a zone of Mg-rich carbonate (possibly dolomite) occurs towards the centre of the pipes, post-dating the calcite cements and in turn being post-dated by equant, drusy mosaic ferroan calcite cements (ec) and/or microcrystalline calcite cement (m2). The QEMSCAN® analysis shows that nearly 80% of the area of

the measured thin section is composed of carbonate cements (Fig. 6C-D). Diagenetic pyrite forms approximately 0.5% of the area of the measured thin section.

The sediment infills and carbonate cements in the two articulated *'Thyasira' townsendi* specimens from Thyasira Hill, SHI (samples DJ.616.22 and DJ.616.34), and the articulated *'T.' townsendi* specimen (PRI 61054) from SI (Table 1) are petrographically very similar to the samples described above, with sparry to microsparry/micritic calcite cemented silty and peloidal sediment, overgrown with multiple zones of fibrous calcite cements, which grow into the open space in the centre of the articulated valves. These cements in the SI *'T.' townsendi* specimen appear black in colour to the naked eye. The shells of *'T.' townsendi* specimens from SHI are recrystallized to sparry calcite and there is no trace of original microstructures.

The concretions at locality D5.345.2 on SI have similar petrographic characteristics to the SHI KCM samples. Where present, multiple generations of banded and botryoidal fibrous calcite cements (bbc) fill centimetre-scale pipe-like structures within the concretions (Figs. 6B; 7D). The bands of fibrous cement are either of a yellowish colour (ybbc) or are translucent (tbbc); although these phases formed recurrently in places, resulting in an intimate intercalation, the former phase tends to predate the latter. In places adjacent to the walls of the pipes the fibrous cements have been recrystallized (rbbc) to equant calcite (Fig. 7D).

D5.4: Carbonate stable carbon and oxygen isotopes

The $\delta^{13}C$ and $\delta^{18}O$ values for the SHI and SI carbonates fall into two distinct clusters (Table 2, Fig. 8). The SI concretion matrices and fibrous calcite cements, and the fibrous calcite cements from inside articulated bivalves have negative $\delta^{13}C$ values between −58.0 and −24.6‰, and $\delta^{18}O$ values between −2.3 and 2.1‰. The SHI carbonate $\delta^{13}C$ values are less negative, with most clustering between −20.4 and −10.7‰. These include all the fibrous calcite cements, the Thyasira Hill cemented sediment, the micro-sparry calcite cement sample and three of the five sparry calcite cement samples. The other

two sparry calcite cements have $\delta^{13}C$ values that straddle the single analysed *'Thyasira' townsendi* shell value of −4.1‰. The $\delta^{18}O$ values of the SHI carbonates are mostly more negative than the SI carbonates, being between −8.3 and −1.6‰..

D5.5: Molecular fossils and their compound-specific isotopes

The hydrocarbon fraction (Fig. 9A) of the studied sample (Sn1-1) from Thyasira Hill, SHI is predominantly composed of *n*-alkanes ranging from *n*-C_{16} to *n*-C_{31} without a preferential distribution of odd or even chains. The *n*-alkanes maximize at intermediate chain lengths (*n*-C_{22} to *n*-C_{24}) and long chain *n*-alkanes (>*n*-C_{27}) are present only in minor amounts. In addition to the *n*-alkanes, multiple branched alkanes, the so-called isoprenoids, are abundant, although in lesser amounts than the *n*-alkanes. Among the identified isoprenoids are the two head-to-tail linked isoprenoids 2,6,10,14-tetramethylpentadecane (pristane) and 2,6,10,14-tetramethylhexadecane (phytane). The latter compound is co-eluting with the tail-to-tail linked isoprenoid 2,6,11,15-tetramethylhexadecane (crocetane). Crocetane makes up approximately 40% of the mixed crocetane/phytane peak. We identify a second tail-to-tail linked isoprenoid as 2,6,10,15,19-pentamethylicosane (PMI). In addition, trace amounts of the head-to-head linked isoprenoid 3,7,11,15,18,22,26,30-octamethyldotriacontane (acyclic biphytane) are present.

The carboxylic acid fraction of the sample (Fig. 9B) is composed predominantly of *n*-fatty acids (FA) with 12 to 32 carbon atoms. The FA show an odd over even predominance. Short-chain FA maximize at *n*-C_{16} FA. Intermediate and long-chain FA (*n*-C_{20} to *n*-C_{28}) show only slightly varying contents, whereas the chains with 29 or more carbons are only present in trace amounts. Other than the straight-chain FA, short-chain terminally-branched FA were identified, including *iso*-C_{14} FA, *iso*- and *anteiso*-C_{15} FA, and *iso*-C_{16} FA. In addition, α,ω-diacids from C_{16} to C_{26} were identified (Fig. 9B). Isoprenoidal biphytanic diacids with 0 to 2 cyclopentane rings were found in trace amounts, with acyclic and bicyclic biphytanic diacids (40% each of all

biphytanic diacids) predominating over the monocyclic biphytanic diacid (20% of all biphytanic diacids). Other than aliphatic compounds, a series of hopanoic acids were found, ranging from C_{31} to C_{34} and maximizing at C_{32}. All hopanoic acids were present as their 17β(H),21β(H)-isomers. The $\delta^{13}C$ values of all the measured *n*-alkanes (*n*-C_{18} to *n*-C_{26}) revealed values of −27‰ and −26‰; the contents of long-chain *n*-alkanes were too low to measure stable carbon isotopes. The mixed crocetane/phytane peak has a value of −61‰, whereas PMI shows a value of −83‰. Biphytane was not measured for its isotopic composition because of its low concentration in the sample. The $\delta^{13}C$ values of *n*-fatty acids range from −40‰ (*n*-C_{16} FA) to −29‰ (*n*-C_{28} FA). The α,ω-diacids have values of −29‰ (C_{24}-diacid) to −25‰ (C_{18}-diacid). The terminally-branched FA showed the strongest variation in $\delta^{13}C$ values ranging from −57‰ (*anteiso*-C_{15} FA) to −35‰ (*iso*-C_{14} FA). The $\delta^{13}C$ values of the hopanoic acids and biphytanic diacids were not measured because they occurred in very low concentrations.

D6: Interpretations

D6.1: Snow Hill Island carbonate deposits as hydrocarbon seeps

We interpret the deposits of carbonate cemented sediments occurring in the KCM on SHI as having being formed by hydrocarbon seepage, because of their morphology, petrography, organic biomarkers and stable isotope values. The wide variation in size of the deposits, and, in particular, their lack of lateral persistence, is a common feature of modern and fossil hydrocarbon seep deposits (e.g. Han et al., 2004; Agirrezabala et al., 2013). We suggest the increasing thickness of the deposits in the KCM on Spath Peninsula up to the level of Thyasira Hill shows increasing flux of hydrocarbons during the deposition of the KCM, as there is no obvious change in sedimentation rate at the time. This increasing flux presumably explains the local increases in numbers of *'Thyasira' townsendi* specimens in the deposits up-section. The *'Thyasira' townsendi* layers below the first occurrence of carbonate cemented layers may indicate incipient seepage within the basin (see section 6.1).

The $\delta^{13}C$ value from the single analysed *'T.' townsendi* shell from the KCM indicates a carbon source from seawater bicarbonate, and not from hydrocarbons, an interpretation which is consistent with the observation that bivalves largely (but not exclusively; Lartaud et al., 2010) use seawater bicarbonate to build their shells (e.g., McConnaughey and Gillikin, 2008). The early non-ferroan micritic to microsparry calcites in the KCM deposits represent the first seep-related cement phase (m1), which locked up the original sediment porosity, and caused later seep fluid to be channelled into conduits (the pipe-like structures). Within these conduits multiple phases of cementation occurred, dominated by the banded and botryoidal fibrous calcite cements (bbc), a common constituent of many modern (e.g. Feng et al., 2010) and ancient seep limestones (e.g. Savard et al., 1996). Based on comparison with other ancient seep limestones (Buggisch and Krumm, 2005; Peckmann et al., 2007a), it seems likely that the primary mineralogy of this phase was aragonite. The overgrowth of faecal pellets by these cements confirms that they had an early diagenetic, pre-compactional origin within the system. The early micrite and fibrous calcite cements from Thyasira Hill have negative $\delta^{13}C$ values, but are not as low as many other Palaeozoic, Mesozoic, Cenozoic and modern seep carbonate cements (Campbell et al., 2002; Birgel et al., 2006a; Himmler et al., 2008; Haas et al., 2010), and may indicate a greater contribution of thermogenic over biogenic methane in the seep fluids and/or greater admixture of seawater bicarbonate. The former hypothesis has some support from the biomarker results, because the PMI in the bulk sample from Thyasira Hill has only a moderate ^{13}C-depletion (−83‰) unlike PMI in other ancient seep carbonates (Birgel et al., 2006a; Kiel et al., 2013), and may be explained by methanotrophic archaea taking up thermogenic methane rather than biogenic methane, which is more ^{13}C-depleted than the former (cf. Whiticar 1999). This has also been suggested for other ancient seep carbonates (e.g. Kaim et al., 2013).

The presumed ankerite cements intergrown with the fibrous cements in the KCM fluid conduits represent periodic carbonate precipitation from fluids enriched in Fe and Mn. In general ankerite is rare in seep limestones and only few ancient and modern occurrences have been reported (Peckmann et al., 2001; Díaz-del-Río et al., 2003). The sparry ferroan calcite (ec) and

microcrystalline calcite cements (m2) in some of the conduits represent late stage burial cements of uncertain age, probably not derived from hydrocarbons, which filled up any remaining porosity in the conduits centres and elsewhere in the deposits.

Some of the molecular fossils in sample Sn1-1 are indicative of micro-organisms involved in AOM. Those indicative of methanotrophic archaea are the isoprenoids PMI, biphytane, and crocetane, as well as the biphytanic diacids. The mixed crocetane/phytane peak (–61‰) is less ^{13}C-depleted than PMI, which can be explained by variable precursors of phytane including (1) phototrophic organisms (chlorophyll; e.g. Peters et al., 2005 and references therein) and (2) methanotrophic archaea (archaeol; Peckmann and Thiel, 2004 for a review). Biphytane and biphytanic diacids cannot be used with certainty as AOM biomarkers in this study, since no δ^{13}C values are available for these compounds. However, the distribution of biphytanic diacids with 0 to 2 cyclopentane rings resembles the findings in other seep carbonates, where δ^{13}C values were available (Birgel et al., 2008a). Therefore, the biphytanic diacids in sample Sn1-1 were likely also sourced by methanotrophic archaea. Biomarkers for SRB involved in AOM are terminally branched fatty acids, especially *iso*- and *anteiso*-C_{15} FAs. Usually, *anteiso*-C_{15} FA predominates over *iso*-C_{15} FA in *Desulfosarcina* and *Desulfobulbus*, which are the partners of methanotrophic archaea in the three known AOM consortia ANME-1, -2, and -3, respectively (Niemann and Elvert, 2008; Rossel et al., 2011). Interestingly, in case of the SHI seep sample *iso*-C_{15} FA predominates over *anteiso*-C_{15} FA and resembles SRB signatures from non-seep microbialites (e.g. Heindel et al., 2012). The strongest ^{13}C-depletion, though, was observed for *anteiso*-C_{15} FA (–57‰), whereas the other terminally-branched FAs are less ^{13}C-depleted (av. –39‰). This offset most likely points to additional input from other SRB not involved in AOM. Based on the biomarker pattern of the SHI seep sample, the utility of terminally-branched fatty acids as long-lasting molecular fossils of SRB involved in AOM is confirmed for rocks of low to moderate maturity (cf. Birgel et al., 2006a). In the analysed sample, terrigenous organic material is less abundant than marine lipids including short-chain *n*-alkanes and *n*-fatty acids. Even though less abundant, the presence of *n*-C_{27} alkane and *n*-C_{28} fatty acids still indicates moderate input of

terrigenous compounds, most likely derived from leaf waxes, agreeing with the carbon isotopic signatures characteristic of land-derived biomass (−27‰ and −29‰, respectively). Similar isotopic values from α,ω-diacids have been recorded from the Jurassic Beauvoisin seep deposit (Peckmann and Thiel, 2004), and on the basis of compound-specific $\delta^{13}C$ values from these compounds it had been concluded that the source biota were not related to AOM. Further, α,ω-diacids with 22 to 24 carbons were suggested to derive from land plants (cf. Pearson et al., 2005, and discussion therein). The presence of land-derived biomass in the KCM is entirely consistent with the shallow water depositional environment and the presence of wood in the seep carbonates (section 2.1).

D6.2: Hydrocarbon seepage on Seymour Island

Our interpretation of hydrocarbon seepage in the LBF rests on our analyses of the carbonate-cemented concretions at locality D5.345.2 and the carbonate cements in the articulated '*Thyasira' townsendi* and '*Lucina' scotti* specimens (Table 1). These cements are petrographically similar to those of the SHI deposits, but the $\delta^{13}C$ values are considerably lower, which for the values as low as −60‰ indicates a contribution of biogenic methane to their formation (cf. Whiticar 1999; Peckmann and Thiel, 2004). As for the SHI deposits, the presence of abundant fibrous, banded and botryoidal cement in the LBF concretions agrees with carbonate formation at seeps. The observed sequence of a yellow variety of this phase predating a translucent variety mirrors paragenetic sequences of other ancient and modern seep limestones (Peckmann et al., 2002; Himmler et al., 2010). The morphology of many of the carbonate-cemented concretions is reminiscent of trace fossils, such as *Thalassinoides*, so we suggest that they represent animal burrows that acted as preferential pathways for the upward flow of fluids in the sediment, and thus acted as loci for the precipitation of seep carbonate cements (e.g. Peckmann et al., 2002). Similar burrow-fills have been observed in both modern (Fig. 5I; Haas et al, 2010; Wetzel, 2013) and ancient (Campbell, 1992; Peckmann et al., 2007b; Mazumdar et al. 2009) hydrocarbon seep sites, sometimes in the

periphery of more active areas of seepage (e.g., Jenkins et al., 2007). The absence of large-scale seep deposits on SI we interpret as being a consequence of change in the nature of hydrocarbon flux and source in the James Ross Basin during the Maastrichtian (see section 6.1).

The discontinuous layers of *'T.' townsendi*, '*L.' scotti* and *Solemya rossiana* in the LBF on SI could also indicate times of periodic diffuse seepage, as these taxa are putatively chemosymbiotic (see section 6.3) and have congeners that are found at both modern and ancient seep sites (e.g., Kiel 2010b). However, at least at genus level, these taxa are not restricted to this environment, commonly occurring in other organic-rich sediments where there are strong redox zones (e.g. seagrass beds and sewage outfalls; e.g. Taylor and Glover, 2006; Taylor et al., 2008; Dando and Southward, 1986), so their presence cannot be used alone as proof of hydrocarbon seepage in the Maastrichtian sediments.

D6.3: Palaeoecology and taxonomic notes

The high degree of articulation amongst the specimens of '*Thyasira' townsendi*, '*Lucina' scotti* and *Solemya rossiana* in the KCM and LBF, and the ventral surface-down orientation of many of them shows that they are preserved mostly *in-situ* and, and have thus not been reworked. This may be surprising, given the shallow water environment in which they lived (see section 2.1), although they were all infaunal taxa and were likely often entombed in sediments by early seep carbonate cementation. All three bivalve taxa belong to families within which either all (Solemyidae and Lucindae), or some (Thyasiridae), of the living species have symbiotic sulphide-oxidizing bacteria in their gills (Fisher and Childress, 1986; Dando and Southward, 1986; Dando et al., 1986). In the case of the thyasirids, it is the larger species (including the genus *Conchocele*) that have chemosymbionts (Dufour, 2005). Thus, we suggest that '*Thyasira' townsendi*, '*Lucina' scotti* and *Solemya rossiana* had symbionts too, and the association of these species with the seep carbonates in the KCM and LBF is no co-incidence, but indicates the presence of AOM-derived hydrogen sulphide in the Maastrichtian sediments in

the basin. However, the presence of a diversity of 'background' benthic molluscan fauna, both epi- and infauna, associated with the chemosymbiotic taxa in the LBF indicates that environmental conditions in the sediment were not too challenging.

The ammonites associated with the bivalves in the seep deposits in the KCM we think were most likely not members of the seep communities, although we note that Landman et al. (2012) found isotopically light carbon ($\delta^{13}C$ values as low as −13.71‰) in the shells of ammonites from one of the Upper Cretaceous (Campanian) Tepee Buttes seep deposits, which they suggest shows ammonites were functionally part of seep communities in the past, at least at this site.

'*Thyasira' townsendi* specimens from SHI were first described by Weller (1903) and were identified by him as being conspecific with White's (1890) species *Lucina? townsendi* from Cretaceous sediments on St. Paul's and St. Peter's Islands in the Magellan Strait. Wilckens (1910) later suggested that *Lucina? townsendi* White 1890 is not a lucinid and transferred the species to the genus *Thyasira*. However, as noted by Zinsmeister and Macellari (1988) the shell of '*Thyasira' townsendi* is much larger than those of other *Thyasira* species, and in size and shape more resembles species belonging to *Conchocele* (Kamenev et al., 2001; Okutani, 2002; Oliver and Sellanes, 2005), hence our placement of the genus name '*Thyasira'* in quotation marks herein. Similarly, the shell morphology of '*Lucina' scotti* (Wilckens) 1910 does not correspond well to this genus (or to Wilckens' original genus *Phacoides*) and instead the species very likely belongs to the extinct lucinid genus *Nymphalucina* Speden 1970 (Kiel, 2013), that is particularly well known from seeps and shales in the Western Interior Seaway in North America (Speden, 1970; Kauffman, 1996; Kiel, 2013), because of the external characters (Fig. 5J), and the shape of the cardinal teeth that can be seen in some weathered articulated specimens. Further systematic work is planned on these taxa to substantiate these observations.

D7: Discussion

D7.1:Seepage within the James Ross Basin

Our evidence shows that hydrocarbon seepage occurred in the James Ross Basin for a significant period of time during the early to late Maastrichtian. In the early Maastrichtian, during the deposition of the KCM in the present day area Spath Peninsula on SHI, the seepage was apparently more intense and of longer duration, leading to the formation of large carbonate-cemented deposits. The seeping fluids at this time appear to have contained a higher proportion of thermogenic methane over other hydrocarbons, as indicated by the molecular fossil inventory and their compound-specific isotopes in the SHI analysed sample (see section 5.1). By the late Maastrichtian, during the deposition of the LBF on SI, seepage was possibly reduced and occurred only periodically, allowing the formation of communities of chemosymbiotic bivalves and with, at one horizon, carbonated-cemented burrows, but not of large seep deposits. These seep fluids probably had a larger contribution of biogenic methane.

There is additional evidence for hydrocarbon seepage at other times and elsewhere in the James Ross Basin area. There are unstudied deposits in the HCM on the Spath Peninsula on SHI and Cape Lamas on SI (Fig. 1) that look similar to those in the KCM, also weathering out from the enclosing sediments, and could thus well be additional seep deposits. Further, stable isotopic studies of calcite cemented concretions from sediments of the Santa Marta Formation (Santonian to Campanian) from northern James Ross Island (Pirrie and Marshall, 1991) and the Maastrichtian aged Sandwich Bluff Member on Vega Island (Pirrie et al., 1994) found a sub-group of concretions preferentially forming within *Planolites* and *Thalassinoides* burrow networks with $\delta^{13}C$ values of −30.4 to −39.2‰ (n=3). They interpreted these values to reflect carbon sourced from sulphate reduction and/or methane oxidation (Pirrie and Marshall, 1991). High Mg calcite fibrous fringing cements also occur within the Eocene La Meseta Formation sediments on SI where they infill *Teredolites* borings in fossil wood (Pirrie et al., 1998). The $\delta^{13}C$ values of these cements varied between 1.7 and −42.6‰, although most values were between −10 and

−40‰. Pirrie et al. (1998) interpreted the carbon source for these cements as coming from methane oxidation.

Thus, hydrocarbon seepage may have occurred within James Ross Basin from the early Maastrichtian through to the Eocene. The source of the hydrocarbons probably varied over this time period, with biogenic methane being derived from the degradation of organic material, including of terrigenous origin (section 5.1) in shallow sediments, and thermogenic methane forming deeper in the sediment pile during intrusion of the arc-related igneous rocks and making its way to the surface by diffusion, or possibly via faults within the basin, for which, however, there is little evidence at outcrop.

D7.2: Maastrichtian seeps: macroevolutionary considerations

The James Ross Basin is only the third published area of Maastrichtian hydrocarbon seepage (the others being the slightly older Tepee Buttes from the Western Interior Basin, USA, and potentially the poorly dated Sada Limestone from Japan). Compared to most other ancient and modern seep communities, the seep fauna of the James Ross Basin is of very low diversity, being dominated by one species (‘*Thyasira’ townsendi*), together with smaller numbers of *Solemya rossiana* and (on SI) ‘*Lucina’ scotti*, all of which probably had thiotrophic chemosymbionts. At present it seems unlikely that any these three taxa were seep obligates, because both ‘*L.’ scotti* (commonly) and *S. rossiana* (rarely) occur throughout the LBF (Zinsmeister and Macellari, 1988), and the type location of ‘*T.’ townsendi* on the St. Paul’s and St. Peter’s Islands has not, to our knowledge, been investigated for the presence of seeps. It is worth noting here that large thyasirid bivalves with very similar morphologies to ‘*T.’ townsendi* are found in other Cretaceous deposits in the high Southern latitudes, including specimens from Deception Island, Antarctica (Figure 5I) and the species *T. bullpointensis* (Stilwell 1994) from North Island, New Zealand.

Absent from the James Ross Basin seep fauna are ‘typical’ obligate seep taxa from the Cretaceous (e.g. *Paskentana*, hokkaidoconchids, *Peregrinella*, and *Caspiconcha*), and the Cenozoic (e.g. vesicomyids and bathymodiolins).

There are a number of possible explanations for this observation. The first relates to evolutionary history of the obligate seep taxa. The oldest discovered vesicomyids and bathymodiolins are Eocene in age (Amano and Kiel, 2007; Kiel and Amano, 2013), whilst the youngest known representatives of *Paskentana*, *Peregrinella* and *Caspiconcha* are from the Hauterivian (*Paskentana* and *Peregrinella*), and Campanian (*Caspiconcha*) (Campbell and Bottjer, 1995; Kiel et al., 2008; Kaim et al., 2008; Jenkins et al., 2013). Thus, the James Ross Basin seep fauna may be both too young to contain representatives of the obligate Mesozoic seep taxa and too old to contain those from the Cenozoic. However, it is worth pointing out here that quite a few obligate seep taxa that ranged from the Cretaceous into the Eocene and younger (such as the gastropods *Ascheria*, *Provanna, Desbruyeresia, Humptulipsia*, *Retiskenea, Serradonta* and *Bathyacmaea*; e.g. Kaim et al., 2014), are all missing from the James Ross Basin seeps.

The second possible explanation is palaeolatitudinal. Perhaps Cretaceous high latitude seep faunas were different from contemporary low latitude faunas, as is the case for non-seep communities (Raup and Jablonski, 1993). Negating this hypothesis is that some typical obligate seep taxa are known from high latitude seep sites, both modern and fossil. Examples are the vesicomyids from modern Larsen B seep sites (Domack et al., 2005), hokkaidoconchids from the Late Jurassic Alexander Island seep (Kaim and Kelly, 2009) and *Caspiconcha* from the Lower Cretaceous Greenland seeps (Kelly et al., 2000). The third possible explanation is related to bathymetry. Modern seeps <200 m do not contain obligate taxa (Sahling et al., 2003), and Kiel (2010a) found the same bathymetric control in Cenozoic and Mesozoic seep faunas. Lucinids, thyasirids and solemyids occur in both shallow and deep seep communities, both modern and ancient (e.g. Dando, 2010; Majima et al., 2005; Kiel et al., 2012), so the occurrence of these taxa in James Ross Basin seeps and the absence of any typical seep obligate fauna may have been related solely to the fact that the James Ross Basin seeps occurred in a shallow shelf setting, most probably shallower than 200 metres. Other similar shallow water fossil examples are the Late Cretaceous Teepee Buttes seeps, the core facies of which are dominated by *Nymphalucina occidentalis* (although the total fauna are considerably more diverse than the James Ross

Basin seep fauna; Kiel et al., 2012, Kaufmann et al., 1996), the Eocene to Holocene Type III seeps of Majima et al. (2005) from Japan (those dominated by *Lucinoma* and/or *Conchocele* and characterised by autochthonous occurrences in muddy sediments from depths of less than 300 m), and the large lucinids (genus *Monitilora*?) from Late Miocene seeps from Taiwan (Chien et al., 2012).

A fourth possible explanation for the absence in the James Ross Basin seeps of 'typical' Cretaceous obligate seep taxa is ecological. Perhaps seepage in the basin was never vigorous enough for sulphide to reach the seafloor, preventing the settlement of obligate epifauna, such as the gastropod taxa listed above, but still supporting infaunal chemosymbiotic bivalve taxa.

D8: Acknowledgments

DB and JP would like to thank Enno Schefuß and Xavier Prieto at the MARUM in Bremen for their help in compound-specific carbon isotope measurements. SK thanks Greg Dietl and Judith Nagel-Myers (Ithaca, NY) for access to the PRI collection and their hospitality during his visit to the PRI. CTSL thanks Laura Tilley for identifying fossil wood fragments in the SHI seep thin sections. JDW thanks James Crampton and Alan Beu (GNS Science, Wellington, New Zealand) for useful discussion and access to fossil collections in their care. Simon Lomas collected some of the material from Snow Hill Island while employed at BAS. We thank Andrzej Kaim and an anonymous reviewer for suggesting improvements to the original version of this paper.

D9: References

Agirrezabala, L.M., Kiel, S., Blumenberg, M., Schäfer, N., Reitner, J., 2013. Outcrop analogues of pockmarks and associated methane-seep carbonates: a case study from Lower Cretaceous (Albian) of the Basque-Cantabrian Basin, western Pyrenees. Palaeogeography, Palaeoclimatology, Palaeoecology 390, 94–115.

Aloisi, G., Pierre, C., Rouchy, J.-M., Foucher, J.-P., Woodside, J., 2000. Methane-related authigenic carbonates of eastern Mediterranean Sea mud volcanoes and their possible relation to gas hydrate destabilization. Earth and Planetary Science Letters 184, 321–338.

Amano, K., Kiel, S., 2007. Fossil vesicomyid bivalves from the North Pacific region. The Veliger 49, 270–293.

Amano, K., Jenkins, R.G., Aikawa, M., Nobuhara, T., 2010. A Miocene chemosynthetic community from the Ogaya Formation in Joetsu: evidence for depth-related ecologic control among fossil seep communities in the Japan Sea back-arc basin. Palaeogeography, Palaeoclimatology, Palaeoecology 286, 164–170.

Baco, A.R., Rowden, A.A., Levin, L.A., Smith, C.R., Bowden, D.A., 2010. Initial characterization of cold seep faunal communities on the New Zealand Hikurangi margin. Marine Geology 272, 251–259.

Birgel, D., Peckmann, J., Klautzsch, S., Thiel, V., Reitner, J., 2006a. Anaerobic and aerobic oxidation of methane at Late Cretaceous seeps in the Western Interior Seaway, USA. Geomicrobiology Journal 23, 565–577.

Birgel, D, Thiel, V., Hinrichs, K.-U., Elvert, M., Campbell, K. A., Reitner, J., Farmer, J. D., Peckmann J., 2006b. Lipid biomarker patterns of methane-seep microbialites from the Mesozoic convergent margin of California. Organic Geochemistry 37, 1289–1302.

Birgel, D., Elvert, M., Han, X., Peckmann, J., 2008a. ^{13}C-depleted biphytanic diacids as tracers of past anaerobic oxidation of methane. Organic Geochemistry 39, 152–156.

Birgel, D, Himmler, T., Freiwald, A., Peckmann, J., 2008b. A new constraint on the antiquity of anaerobic oxidation of methane: Late Pennsylvanian seep limestones from southern Namibia. Geology 36, 543–546.

Boetius, A., Ravenschlag, K., Schubert, C.J., Rickert, D., Widdel, F., Gieseke, A., Amann, R., Jørgensen, B.B., Witte, U., Pfannkuche, O., 2000. A marine microbial consortium apparently mediating anaerobic oxidation of methane. Nature 407, 623–626.

Bouloubassi, I., Aloisi, G., Pancost, R., Hopmans, E., Pierre, C., Sinninghe Damsté, J.S., 2006. Archaeal and bacterial lipids in authigenic carbonate crusts from eastern Mediterranean mud volcanoes. Organic Geochemistry 37, 484–500.

Bowman, V.C., Francis, J.E., Riding, J.B., Hunter, S.J., Haywood, A.M., 2012. A latest Cretaceous to earliest Paleogene dinoflagellate cyst zonation from Antarctica, and implications for phytoprovincialism in the high southern latitudes. Review of Palaeobotany and Palynology 171, 40–56.

Bowman, V.C., Francis, J.E., Riding, J.B. 2013. Late Cretaceous winter sea ice in Antarctica? Geology 41, 1227–1230.

Buggisch, W., Krumm, S., 2005. Palaeozoic cold seep carbonates from Europe and North Africa – an integrated isotopic and geochemical approach. Facies 51, 566–583.

Campbell, K.A., 1992. Recognition of a Mio-Pliocene cold seep from the northeast Pacific convergent margin, Washington, U.S.A. Palaios 7, 422–433.

Campbell, K.A., 2006. Hydrocarbon seep and hydrothermal vent paleonvironments and paleontology: past developments and future research directions. Palaeogeography, Palaeoclimatology, Palaeoecology 232, 362–407.

Campbell, K.A., Bottjer, D.J., 1995. *Peregrinella*: an Early Cretaceous cold-seep restricted brachiopod. Paleobiology 21, 461–478.

Campbell, K.A, Farmer, J.D., Des Marais, D., 2002. Ancient hydrocarbon seeps from the Mesozoic convergent margin of California: carbonate geochemistry, fluids and palaeoenvironments. Geofluids 2, 63–94.

Charrier, R., Lahsen, A., 1968. Stratigraphy of Late Cretaceous-Early Eocene, Seno Skyring-Strait of Magellan Area, Magallanes Province, Chile. The American Association of Petroleum Geologists Bulletin 53, 568–590.

Chien, C.W., Huang, C.Y., Chen, Z., Lee, H.C., Harris, R. 2012. Miocene shallow-marine cold seep carbonate in fold-and-thrust Western Foothills, SW Taiwan. Journal of Asian Earth Sciences 56, 200–211.

Cordes, E.E., Carney, S.L., Hourdez, S., Carney, R.S., Brooks, J.M., Fisher, C.R., 2007. Cold seeps of the deep Gulf of Mexico: community structure and biogeographic comparisons to Atlantic equatorial belt seep communities. Deep-Sea Research I 54, 637–653.

Craig, H., 1957. Isotopic standards and isotopic correction factors for mass spectrometric analysis of carbon dioxide. Geochimica Cosmochimica Acta 12, 133–149.

Crame, J.A., Francis, J.E., Cantrill, D.J., Pirrie, D., 2004. Maastrichtian stratigraphy of Antarctica. Cretaceous Research 25, 411–423.

Crame, J.A., Lomas, S.A., Pirrie, D., Luther, A., 1996. Late Cretaceous extinction patterns in Antarctica. Journal of the Geological Society of London 153, 503–506.

Crame, J.A., Luther, A., 1997. The last inoceramid bivalves in Antarctica. Cretaceous Research 18, 179–195.

Crame, J.A., McArthur, J.M., Pirrie, D., Riding, J.B., 1999. Strontium isotope correlation of the basal Maastrichtian stage in Antarctica to the European and US biostratigraphic schemes. Journal of the Geological Society of London 156, 957–964.

Dando, P.R., 2010. Biological communities at marine shallow-water seep and vent sites. In: S. Kiel (Editor), The Vent and Seep Biota. Topics in Geobiology. Springer, Heidelberg, pp. 333–378.

Dando, P.R., Southward, A.J., 1986. Chemoautotrophy in bivalve molluscs of the genus *Thyasira*. Journal of the Marine Biological Association of the U.K. 66, 915–929.

Dando, P.R., Southward, A.J., Southward, E.C., 1986. Chemoautotrophic symbionts in the gills of the bivalve mollusc *Lucinoma borealis* and the sediment chemistry of its habitat. Proceedings of the Royal Society of London, B 227, 227–247.

Díaz-del-Río, V., Somoza, L., Martínez-Frias, J., Mata, M.P., Delgado, A., Hernandez-Molina, F.J., Lunar, R., Martín-Rubí, J.A., Maestro, A., Fernández-Puga, M.C., León, R., Llave, E. Medialdea, T., Vázquez, J.T., 2003. Vast fields

of hydrocarbon-derived carbonate chimneys related to the accretionary wedge/olistostrome of the Gulf of Cádiz. Marine Geology 195, 177–200.

Dingle, R.V., 1995. Report of fieldwork undertaken in the Snow Hill Island-James Ross Island area and around Low Head, King George Island: December 1994-February 1995. British Antarctic Survey unpublished field report, R/1994/GL1.

Domack, E., Ishman, S., Leventer, A., Sylva, S., Willmott, V., Huber, B., 2005. A chemotrophic ecosystem found beneath Antarctic ice shelf. Eos, 86, 269–276.

Dubilier, N., Bergin, C., Lott, C., 2008. Symbiotic diversity in marine animals: the art of harnessing chemosynthesis. Nature Reviews Microbiology 6, 725–740.

Dufour, S.C., 2005. Gill anatomy and the evolution of symbiosis in the bivalve family Thyasiridae. Biological Bulletin 208, 200–212.

Dutton, A., Huber, B.T., Lohmann, K. C., Zinsmeister, W.J., 2007. High-resolution stable isotope profiles of a dimitobelid belemnite: implications for paleodepth habitat and late Maastrichtian climate seasonality. Palaios 22, 642-650.

Elvert, M., Greinert, J., Suess, E., Whiticar, M.J., 2000. Archaea mediating anaerobic methane oxidation in deep-sea sediments at cold seeps of the eastern Aleutian subduction zone. Organic Geochemistry 31, 1175–1187.

Feng, D., Chen, D., Peckmann, J., Bohrmann, G., 2010. Authigenic carbonates from methane seeps of the northern Congo fan: Microbial formation mechanism. Marine and Petroleum Geology 27, 748–756.

Fisher, C.R., Childress, J.J., 1986. Translocation of fixed carbon from symbiotic bacteria to host tissues in the gutless bivalve *Solemya reidi*. Marine Biology 93, 59–68.

Friedrich, O., Norris, R.D., Erbacher, J., 2012. Evolution of middle to Late Cretaceous oceans – A 55 m.y. record of Earth's temperature and carbon cycle. Geology 40, 107–110.

Gardin, S., Galbrun, B., Thibault, N., Coccioni, R., Premoli-Silva, I., 2012. Bio-magnetochronology for the upper Campanian - Maastrichtian from the Gubbio area, Italy: new results from the Contessa Highway and Bottaccione sections. Newsletters on Stratigraphy 45, 75–103.

Goedert, J.L., Squires, R.L., 1990. Eocene deep-sea communities in localized limestones formed by subduction-related methane seeps, southwestern Washington. Geology 18, 1182–1185.

Haas, A., Peckmann, J., Elvert, M., Sahling, H., Bohrmann, G., 2010. Patterns of carbonate authigenesis at the Kouilou pockmarks on the Congo deep-sea fan. Marine Geology 268, 129–136.

Han, X., Suess, E., Sahling, H., Wallmann, K., 2004. Fluid venting activity on the Costa Rica margin: new results from authigenic carbonates. International Journal of Earth Sciences 93, 596–611.

Heindel, K., Birgel, D., Brunner, B., Thiel, V., Westphal, H., Gischler, E., Ziegenbalg, S.B., Cabioch, G., Sjövall, P., Peckmann, J., 2012. Post-glacial microbialite formation in coral reefs of the Pacific, Atlantic, and Indian Oceans. Chemical Geology 304–305, 117–130.

Henderson, R.A., 1970. Ammonoidea from the Mata Series (Santonian – Maastrichtian) of New Zealand. Special Papers in Palaeontology 6, 82p.

Henderson, R.A., McNamara, K.J., 1985. Maastrichtian non-heteromorph ammonites from the Miria Formation, Western Australia. Palaeontology 28, 35–88.

Himmler, T., Bach, W., Bohrmann, G., Peckmann, J., 2010. Rare earth elements in authigenic methane-seep carbonates as tracers for fluid composition during early diagenesis. Chemical Geology 277, 126–136.

Himmler, T., Freiwald, A., Stollhofen, H., Peckmann, J., 2008. Late Carboniferous hydrocarbon-seep carbonates from the glaciomarine Dwyka Group, southern Namibia. Palaeogeography, Palaeoclimatology, Palaeoecology 257, 185–197.

Hinrichs, K.-U., Hayes, J.M., Sylva, S.P., Brewer, P.G., DeLong, E.F., 1999. Methane-consuming archaebacteria in marine sediments. Nature 398, 802–805.

Husson, D., Galbrun, B., Laskar, J., Hinnov, L., Thibault, N., Gardin, S., Locklair, R.E., 2011. Astronomical calibration of the Maastrichtian (late Cretaceous). Earth and Planetary Science Letters 305, 328–340.

Jenkins, R.G., Kaim, A., Little, C.T.S., Iba, Y., Tanabe, K., Campbell, K.A., 2013. Worldwide distribution of modiomorphid bivalve genus *Caspiconcha* in late Mesozoic hydrocarbon seeps. Acta Palaeontologica Polonica 58, 357–382.

Jenkins, R.G., Kaim, A., Hikida, Y., Tanabe, K., 2007. Methane-flux-dependent lateral faunal changes in a Late Cretaceous chemosymbiotic assemblage fromthe Nakagawa area of Hokkaido, Japan. Geobiology 5, 127–139.

Judd, A., Hovland, M., 2009. Seabed Fluid Flow. Cambridge University Press. 492 pp.

Kaim, A., Kelly, S.R.A., 2009. Mass occurrence of hokkaidoconchid gastropods in the Upper Jurassic methane seep carbonate from Alexander Island, Antarctica. Antarctic Science 21, 279–284.

Kaim, A., Jenkins, R.G., Warén, A., 2008. Provannid and provannid-like gastropods from the Late Cretaceous cold seeps of Hokkaido (Japan) and the fossil record of the Provannidae (Gastropoda: Abyssochrysoidea). Zoological Journal of the Linnean Society 154, 421–436.

Kaim, A., Skupien, P., Jenkins, R.G., 2013. A new Lower Cretaceous hydrocarbon seep locality from the Czech Carpathians and its fauna. Palaeogeography, Palaeoclimatology, Palaeoecology 390, 42–51.Kaim, A., Jenkins, R.G., Tanabe, K., Kiel, S., 2014. Mollusks from late Mesozoic seep deposits, chiefly in California. Zootaxa 3861, 401–440.

Kamenev, G.M., Nadtochy, V.A., Kuznetsov, A.P., 2001. *Conchocele bisecta* (Conrad, 1849) (Bivalvia: Thyasiridae) from cold-water methane-rich areas of the Sea of Okhotsk. The Veliger 44, 84–94.

Kauffman, E.G., Arthur, M.A., Howe, B., Scholle, P.A., 1996. Widespread venting of methane-rich fluids in Late Cretaceous (Campanian) submarine springs (Tepee Buttes), Western Interior seaway, U.S.A. Geology 24, 799–802.

Kelly, S.R.A., Blanc, E., Price, S.P., Withham, A.G., 2000. Early Cretaceous giant bivalves from seep-related limestone mounds, Wollaston Forland, Northeast Greenland. In: Harper, E.M., Taylor, J.D., Crame, J.A. (Eds.), The Evolutionary Biology of the Bivalvia: Geological Society, London, Special Publications, 177, pp. 227–246.

Kennedy, W.J., Crame, J.A., Bengtson, P., Thompson, M.R.A., 2007. Coniacian ammonites from James Ross Island, Antarctica. Cretaceous Research 28, 509–531.

Kennedy, W.J., Klinger, H.C., 1985. Cretaceous faunas from Zululand and Natal, South Africa. The ammonite family Kossmaticeratidae Spath, 1922. Annals of the South African Museum 95, 165–231.

Kiel, S., 2010a. On the potential generality of depth-related ecologic structure in cold-seep communities: Evidence from Cenozoic and Mesozoic examples. Palaeogeography, Palaeoclimatology, Palaeoecology 295, 245–257.

Kiel, S., 2010b. The fossil record of vent and seep mollusks. In: S. Kiel (Editor), The Vent and Seep Biota. Topics in Geobiology. Springer, Heidelberg, pp. 255–278.

Kiel, S., 2013. Lucinid bivalves from ancient methane seeps. Journal of The Malacological Society of London 79, 346–363.

Kiel, S., Amano, K., 2013. The earliest bathymodiolin mussels: An evaluation of Eocene and Oligocene taxa from deep-sea methane seep deposits in Western Washington State, USA. Journal of Paleontology 87, 589–602.

Kiel, S., Little, C.T.S., 2006. Cold seep mollusks are older than the general marine mollusk fauna. Science 313, 1429–1431.

Kiel, S., Birgel, D., Campbell, K.A., Crampton, J.S., Schiøler, P., Peckmann, J., 2013. Cretaceous methane-seep deposits from New Zealand and their fauna. Palaeogeography, Palaeoclimatology, Palaeoecology 390, 17–34.

Kiel, S., Campbell, K.A., Elder, W.P., Little, C.T.S., 2008. Jurassic and Cretaceous gastropods from hydrocarbon-seeps in forearc basin and accretionary prism settings, California. Acta Palaeontologica Polonica 53, 679–703.

Kiel, S., Wiese, F., Titus, A.L., 2012. Shallow-water methane-seep faunas in the Cenomanian Western Interior Seaway: No evidence for onshore-offshore adaptations to deep-sea vents. Geology 40, 839–842.

Landman, N.H., Cochran, J.K., Larson, N.L., Brezina, J., Garb, M.P., Harries, P.J., 2012. Methane seeps as ammonite habitats in the U.S. Western Interior Seaway revealed by isotopic analyses of well-preserved shell material. Geology 40, 507–510.

Lartaud, F., de Rafelis, M., Oliver, G., Krylova, E., Dyment, J., Ildefonse, B., Thibaud, R., Gente, P., Hoisé, E., Meistertzheim, A.L., Fouquet, Y., Gaill F., Le Bris, N., 2010. Fossil clams from a serpentinite-hosted sedimented vent field near the active smoker complex Rainbow (MAR, 26°13N): insight into the biogeography of vent fauna. Geochemistry Geophysics Geosystems 11, Q0AE01.

Levin, L.A., 2005. Ecology of cold seep sediments: interactions of fauna with flow, chemistry and microbes. Oceanography and Marine Biology. Annual Review 43, 1–46.

Levin, L.A., James, D.W., Martin, C.M., Rathburn, A.E., Harris, L.H., Michener, R.H., 2000. Do methane seeps support distinct macrofaunal assemblages? Observations on community structure and nutrition from the northern California slope and shelf. Marine Ecology Progress Series 208, 21–39.

Lomas, S.A., 1995. Sedimentological and stratigraphic studies of Snow Hill Island, 1994/95. British Antarctic Survey unpublished field report, R/1994/GL5.

Macellari, C.E., 1986. Late Campanian-Maastrichtian ammonite fauna from Seymour Island (Antarctic Peninsula). Memoir (The Paleontological Society) 18, 1–55

Majima, R., Nobuhara, T., Kitazaki, T., 2005. Review of fossil chemosynthetic assemblages in Japan. Palaeogeography, Palaeoclimatology, Palaeoecology 227, 86–123.

Mazumdar, A., Joshi, R.K., Peketi, A., Kocherla, M., 2011. Occurrence of faecal pellet-filled simple and composite burrows in cold seep carbonates: a glimpse of a complex benthic ecosystem. Marine Geology 289, 117–121.

McArthur, J.M., Thirlwall, M.F., Engkilde, M., Zinsmeister, W.J., Howarth, R.J., 1998. Strontium isotope profiles across K/T boundary sequences in Denmark and Antarctica. Earth and Planetary Science Letters 160, 179–192.

McArthur, J.M., Crame, J.A., Thirlwall, J.E., 2000. Definition of Late Cretaceous stage boundaries in Antarctica using strontium isotope stratigraphy Journal of Geology 108, 623–640.

McConnaughey, T.A., Gillikin, D.P., 2008. Carbon isotopes in mollusk shell carbonates, Geo-Marine Letters 28, 287–299.

Metz, C.L., 2010. Tectonic controls on the genesis and distribution of Late Cretaceous, Western Interior Basin hydrocarbon-seep mounds (Tepee Buttes) of North America. Journal of Geology 118, 201–213.

Naehr, T.H., Eichhubl, P., Orphan, V.J., Hovland, M., Paull, C.K., Ussler III, W., Lorenson, T.D., Greene, H.G., 2007. Authigenic carbonate formation at hydrocarbon seeps in continental margin sediments: a comparative study. Deep-Sea Research II 54,1268–1291.

Niemann, H., Elvert, M., 2008. Diagnostic lipid biomarker and stable carbon isotope signatures of microbial communities mediating the anaerobic oxidation of methane with sulphate. Organic Geochemistry 39, 1668–1677.

Niemann, H., Fischer, D., Graffe, D., Knittel, K., Montiel, A., Heilmayer, O., Nöthen, K., Pape, T., Kasten, S., Bohrmann, G., Boetius, A., Gutt, J., 2009. Biogeochemistry of a low-activity cold seep in the Larsen B area, western Weddell Sea, Antarctica. Biogeosciences 6, 2383–2395.

Nobuhara, T., Onda, D., Kikuchi, N., Kondo, Y., Matsubara, K., Amano, K., Jenkins, R.G., Hikida, Y., Majima, R., 2008. Lithofacies and fossil assemblages of the Upper Cretaceous Sada Limestone, Shimanto City, Kochi Prefecture, Shikoku, Japan. Fossils, The Palaeontological Society of Japan 84, 47–60.

Okutani, T., 2002. A new thyasirid *Conchocele novaeguinensis* n. sp. from a thanatocoenosis associated with a possible cold seep activity off New Guinea. Venus, 61, 141–145.

Oliver, P.G., Killeen, I.J., 2002. The Thyasiridae (Mollusca: Bivalvia) of the British continental shelf and North Sea oilfields. An identification manual.

Studies in Marine Biodiversity and Systematics from the National Museum of Wales. BIOMÔR Reports 3, 1–73.

Oliver, P.G., Sellanes, J., 2005. New species of Thyasiridae from a methane seepage area off Concepción, Chile. Zootaxa 1092, 1–20.

Olivero, E.B., 1984. Nuevos amonites Campanianos de la Isla James Ross, Antartida. Ameghiniana 21, 53–84.

Olivero, E.B., 1988. Early Campanian heteromorph ammonites from James Ross Island, Antarctica. National Geographic Research 4, 259–271.

Olivero, E.B., 1992. Asociaciones de Amonites de la Formacion Santa Marta (Cretacico Tardio), Isla James Ross, Antartida. In: C.A. Rinaldi (Ed.), Geología de la Isla James Ross, Instituto Antártico Argentino, Buenos Aires (1992), 47–76.

Olivero, E.B., 2012. Sedimentary cycles, ammonite diversity and palaeoenvironmental changes in the Upper Cretaceous Marambio Group, Antarctica. Cretaceous Research 34, 348–366.

Olivero, E.B., Medina, F.A., 2000. Patterns of Late Cretaceous ammonite biogeography in southern high latitudes: the family Kossmaticeratidae in Antarctica. Cretaceous Research 21, 269–279.

Olivero, E.B., Ponce, J.J., Martinioni, D.R., 2008. Sedimentology and architecture of sharp-based tidal sandstones in the upper Marambio Group, Maastrichtian of Antarctica. Sedimentary Geology 210, 11–26.

Paull, C.K., Hecker, B., Commeau, R., Freeman-Lynde, R.P., Neumann, C., Corso, W.P., Golubic, S., Hook, J.E., Sikes, E., Curray, J., 1984. Biological communities at the Florida Escarpment resemble hydrothermal vent taxa. Science 226, 965–967.

Pearson, M.J., Hendry, J.P., Taylor, C.W., Russell, M.A., 2005. Fatty acids in sparry calcite fracture fills and microsparite cement of septarian diagenetic concretions. Geochimica et Cosmochimica Acta 69, 1773–1786.

Peckmann, J., Thiel, V., 2004. Carbon cycling at ancient methane-seeps. Chemical Geology 205, 443–467.

Peckmann, J., Campbell, K.A., Walliser, O.H., Reitner, J., 2007a. A Late Devonian hydrocarbon-seep deposit dominated by dimerelloid brachiopods, Morocco. Palaios 22, 114–122.

Peckmann, J., Gischler, E., Oschmann, W., Reitner, J., 2001. An Early Carboniferous seep community and hydrocarbon-derived carbonates from the Harz Mountains, Germany. Geology 29, 271–274.

Peckmann, J., Goedert, J.L., Thiel, V., Michaelis, W., Reitner, J., 2002. A comprehensive approach to the study of methane-seep deposits from the Lincoln Creek Formation, western Washington State, USA. Sedimentology 49, 855–873.

Peckmann, J., Senowbari-Daryan, B., Birgel, D., Goedert, J.L., 2007b. The crustacean ichnofossil *Palaxius* associated with callianassid body fossils in an Eocene methane-seep limestone, Humptulips Formation, Olympic Peninsula, Washington. Lethaia 40, 273–280.

Peckmann, J., Thiel, V., Michaelis,W., Clari, P., Gaillard, C., Martire, L., Reitner, J., 1999. Cold seep deposits of Beauvoisin (Oxfordian, southeastern France) and Marmorito (Miocene, northern Italy): microbially induced authigenic carbonates. International Journal of Earth Sciences 88, 60–75.

Peters, K.E., Walters, C.C., Moldowan, J. M., 2005. The Biomarker Guide. Cambridge University Press (1155 pp.).

Pirrie, D., Marshall, J.D., 1990. High paleolatitide Late Cretaceous paleotemperatures: new data from James Ross Island, Antarctica. Geology 18, 31–34.

Pirrie, D., Marshall, J.D., 1991. Field relationships and stable isotope geochemistry of concretions from James Ross Island, Antarctica. Sedimentary Geology 71, 137–150.

Pirrie, D., Ditchfield, P.W., Marshall, J.D., 1994. Burial diagenesis and pore-fluid evolution in a Mesozoic back-arc basin: the Marambio Group, Vega Island, Antarctica. Journal of Sedimentary Research 64, 541–552.

Pirrie, D., Crame, J.A., Lomas, S.A., Riding, J.B. 1997. Late Cretaceous stratigraphy of the Admiralty Sound region, James Ross Basin, Antarctica. Cretaceous Research 18, 109–137.

Pirrie, D., Marshall, J.D., Crame, J.A., 1998. Marine high Mg calcite cements in *Teredolites*-bored fossil wood; evidence for cool paleoclimates in the Eocene La Meseta Formation, Seymour Island, Antarctica. Palaios 13, 276–286.

Pirrie, D., Butcher, A.R., Power, M.R., Gottlieb, P., Miller, G.L., 2004. Rapid quantitative mineral and phase analysis using automated scanning electron microscopy (QemSCAN); potential applications in forensic geoscience. In Pye, K. & Croft, D.J. (eds) Forensic Geoscience: Principles, Techniques and Applications. Geological Society, London, Special Publication 232, 123–136.

Pirrie, D., Rollinson, G.K., Andersen, J.A., Wootton, D., Moorhead, S., 2014. Soil forensics as a tool to test reported artefact find sites. Journal of Archaeological Science 41, 461–473.

Raup, D.M., Jablonski, D., 1993. Geography of end-Cretaceous marine bivalve extinctions. Science 260, 971–973.

Reitner, J., Peckmann, J., Blumenberg, M., Michaelis, W., Reimer, A., Thiel, V., 2005. Concretionary methane-seep carbonates and associated microbial communities in Black Sea sediments. Palaeogeography, Palaeoclimatology, Palaeoecology 227, 18–30.

Ritger, S., Carson, B., Suess, E., 1987. Methane-derived authigenic carbonates formed by subduction-induced pore-water expulsion along the Oregon/Washington margin. Geological Society of America Bulletin 98, 147–156.

Rossel, P.E., Elvert, M., Ramette, A., Boetius, A., Hinrichs, K.-U., 2011. Factors controlling the distribution of anaerobic methanotrophic communities in marine environments: Evidence from intact polar membrane lipids. Geochimica et Cosmochimica Acta 75, 164–184.

Sahling, H., Galkin, S.V., Salyuk, A., Greinert, J., Foerstel, H., Piepenburg, D., Suess, E., 2003. Depth-related structure and ecological significance of cold-seep communities – a case study from the Sea of Okhotsk. Deep-sea Research I 50, 1391–1409.

Salazar, C., Stinnesbeck, W., Qunzio-Sinn, L.A., 2010. Ammonites from the Maastrichtian (Upper Cretaceous) Quiriquina Formation in central Chile. Neues Jahrbuch für Geologie und Paläontologie 257, 181–236.

Savard, M.M., Beauchamp, B., Veizer, J., 1996. Significance of aragonite cements around Cretaceous marine methane seeps. Journal of Sedimentary Research 66, 430–328.

Schwartz, H., Sample, J., Weberling, K.D., Minisini, D., Moore, J.C., 2003. An ancient linked fluid migration system: Cold-seep deposits and sandstone intrusions in the Panoche Hills, California, USA. Geo-Marine Letters 23, 340–350.

Sellanes, J., Quiroga, E., Gallardo, V.A., 2004. First direct evidence of methane seepage and associated chemosynthetic communities in the bathyal zone off Chile. Journal of the Marine Biological Association of the United Kingdom 84, 1065–1066.

Sibuet, M., Olu, K., 1998. Biogeography, biodiversity and fluid dependence of deep-sea cold-seep communities at active and passive margins. Deep-Sea Research II 45, 517–567.

Speden, I.G., 1970. The type Fox Hills Formation, Cretaceous (Maestrichtian), South Dakota. Part 2. Systematics of the Bivalvia. Peabody Museum of Natural History Yale University, Bulletin 33, 1–222.

Stilwell, J.D., 1994. Latest Cretaceous to earliest Paleogene molluscan faunas of New Zealand: changes in composition as a consequence of break-up of Gondwana and extinction. Unpublished PhD dissertation, University of Otago, Dunedin, 1630 pp, 84 pls.

Stinnesbeck, W., Ifrim, C., Salazar, C., 2012. The last Cretaceous ammonites in Latin America. Acta Palaeontologica Polonica 57, 717–728.

Taylor, J.D., Glover, E.A., 2006. Lucinidae (Bivalvia) - the most diverse group of chemosymbiotic molluscs. Zoological Journal of the Linnean Society, 148, 421–438.

Taylor, J.D., Glover, E.A., Williams, S.T., 2008. Ancient shallow water chemosynthetic bivalves: systematics of Solemyidae from eastern and

southern Australia (Mollusca, Bivalvia). Memoires of the Queensland Museum – Nature 54, 75–104.

Thiel, V., Peckmann, J., Seifert, R., Wehrung, P., Reitner, J., Michaelis, W., 1999. Highly isotopically depleted isoprenoids: molecular markers for ancient methane venting. Geochimica et Cosmochimica Acta 63, 3959–3966.

Tobin, T.S., Ward, P.D., Steig, E.J., Olivero, E.B., Hilburn, I.A., Mitchell., R.D., Diamond, M.R., Raub, T.D., Kirschvink, J.L., 2012. Extinction patterns, $\delta^{18}O$ trends, and magnetostratigraphy from a southern high-latitude Cretaceous-Paleogene section: Links with Deccan volcanism. Palaeogeography, Palaeoclimatology, Palaeoecology 350-352, 180–188.

Voigt, S., Gale, A.S., Jung, C., Jenkyns, H.C., 2012. Global correlation of Upper Campanian - Maastrichtian successions using carbon-isotope stratigraphy: development of a new Maastrichtian timescale. Newsletters on Stratigraphy 45, 25–53.

Walaszczyk, I., Kennedy, W.J., Klinger, H.C., 2009. Cretaceous faunas from Zululand and Natal, South Africa. Systemtic palaeontology and stratigraphical potential of the Upper Campanian-Maastrichtian Inoceramidae (Bivalvia). African Natural History 5, 49–132.

Weller, S., 1903. The Stokes collection of Antarctic fossils. The Journal of Geology 11, 413-419.

Wetzel, A., 2013. Formation of methane-related authigenic carbonates within the bioturbated zone - An example from the upwelling area off Vietnam. Palaeogeography, Palaeoclimatology, Palaeoecology 386, 23–33.

Wilckens, O., 1910. Die Anneliden, Bivalven, und Gastropoden der Antarktischen Kreideformationen. Wissenschaftliche Ergebnisse der Schwedischen Südpolar-Expedition, 1901–1903 3, 1–132.

White, C.A., 1890. On certain Mesozoic fossils from the Islands of St. Paul's and St. Peter's in the Straits of Magellan. Proceedings of the United States National Museum 13, 13–14.

Whiticar, M.J., 1999. Carbon and hydrogen isotope systematics of bacterial formation and oxidation of methane. Chemical Geology 161, 291–314.

Zinsmeister, W.J., 1998. Discovery of fish mortality horizon at the K-T boundary on Seymour Island: Re-evaluation of events at the end of the Cretaceous. Journal of Paleontology 72, 556–571.

Zinsmeister, W.J., Feldmann, R.M., 1996. Late Cretaceous faunal changes in the high southern latitudes: a harbinger of global catastrophe? In: McLeod, N., Keller, G. (Eds.), Biotic and Environmental Events across the Cretaceous/Tertiary Boundary. Norton, New York, NY, 303–326.

Zinsmeister, W.J., Macellari, C.E., 1988. Bivalvia (Mollusca) from Seymour Island, Antarctic Peninsula. In: Feldmann, R.M., Woodburne, M.O. (Eds.), Geology and Paleontology of Seymour Island, Antarctic Peninsula. Geological Society of America Memoirs 169, 253–284.

D10: Figure captions

Fig. 1. (A) Locality map showing outcrops of Marambio Group sediments in the Trinity Peninsula and James Ross Island areas of Antarctica (inset). (B) Outline geological map of Seymour Island and the NE tip of Snow Hill Island; modified from Crame et al. (2004).

Fig. 2. Composite stratigraphy of the Maastrichtian part of the Marambio Group on Snow Hill and Seymour Islands, following Pirrie et al. (1997), Crame et al. (2004) Bowman et al. (2013) for lithostratigraphy and biostratigraphy, and MacArthur et al. (1998), Tobin et al. (2012), and Bowman et al. (2013) for chronostratigraphy. Stars mark the approximate positions of the studied hydrocarbon seep deposits in the stratigraphic column. Black circles indicate other occurrences of the chemosynthetic bivalve assemblage ('*Thyasira*', '*Lucina*', *Solemya*) collected during BAS expeditions. Abbreviations: SHI = Snow Hill Island; KCM = Karlsen Cliffs Member; HCM = Haslum Crag Member; S = Sobral Formation; K = Cretaceous; Pg = Paleogene; Dan = Danian.

Fig. 3. Field images of carbonate cemented sediments and associated fossils from BAS section DJ.616 in the Karlsen Cliffs Member, near Nordenskjold's Hut, Snow Hill Island, looking towards the SW. The section (A) runs from the base of the hill, bottom right of the photograph, up the slope through points where photographs (C-E) were taken, over Thyasira Hill to BAS locality DJ.617. The cliffs at the top left of the photograph (A) are outcrops of the Haslum Crag Member. The white arrow points in the younging direction, perpendicular to the dip of the beds. (B) and (D) Irregularly shaped patches of carbonate cemented sediments. (C) In-situ articulated '*Thyasira' townsendi* specimens in plan view on the surface of an exposed bedding plane. (E) Ammonites and articulated '*Thyasira'townsendi* specimens, base of Thyasira Hill. Geological hammers for scale in (B) (see white arrow), (C), (D) and (E) approximately 40 cm long.

Fig. 4. Field images of carbonate cemented sediments and associated fossils from Karlsen Cliffs Member, Snow Hill Island. (A) Thyasira Hill; arrow shows position of image (C). (B) Knolls of exhumed carbonate cemented sediment, approximately 200 m East of Thyasira Hill; arrow shows position of image (D). Outcrops in the hills in background are Haslum Crag Member. (C) Detail of (A) showing carbonate cemented sediment enclosing weathered articulated '*Thyasira' townsendi* specimens; sample Sn1-1 comes from this location. (D) Detail of knoll in (B) with Thyasira Hill in background, to left; arrow points to hammer scale. Geological hammers for scale in (C) and (D) approximately 30 cm long.

Fig. 5. Fossils and carbonate concretions from Snow Hill and Seymour Islands. (A) Hand specimen of carbonated cemented siltstone, sample Sn1-1, Thyasira Hill, Karlsen Cliffs Member, Snow Hill Island. White arrows point to articulated '*Thyasira*' *townsendi* specimens in various sections. Black arrow points to sparry calcite cement patch. Codes 1A and B are sites were matrix samples (Sn1-1a and Sn1-1b respectively) were drilled for stable isotope analysis (see Table 2). This specimen was subsequently destroyed for biomarker analysis. (B) Three cut tubular carbonate concretions from locality D5.345.2, López de Bertodano Formation, Seymour Island. The concretion on the right hand side was sectioned and its exposed centre drilled for stable isotope analysis (sample D5.345.2 a; see Table 2). Note the presence of small *Planolites*-like burrows on the surface of the concretion. (C) Carbonate concretion formed of cemented large burrows with smaller burrows on their surfaces; from Hydrate Hole seep site, 3100 m water depth, Congo deep-sea fan (see Haas et al., 2010 for details); specimen GeoB 8212-1. (D) Ammonite *Maorites seymourianus* from locality D5.347.2, López de Bertodano Formation, Seymour Island. (E) Ammonite *Gunnarites* sp., possibly *Gunnarites bhavaniformis* from locality DJ.633.1, Karlsen Cliffs Member, Snow Hill Island. (F) Ammonite *Jacobites anderssoni* from locality DJ.633.1, Karlsen Cliffs Member, Snow Hill Island. (G) Right valve of articulated specimen of bivalve '*Thyasira' townsendi* from Thyasira Hill, Snow Hill Island; shell material present on umbo and anterior margin. (H) Right valve of articulated specimen of bivalve '*Thyasira' townsendi* from locality D5.345.2, López de Bertodano Formation, Seymour Island; internal mould. (I) Left valve of articulated large thyasirid bivalve from Deception Island, Antarctica; Paleontological Research Institution 1464. (J) Right valve of articulated specimen of bivalve *'Lucina' scotti*, Paleontological Research Institution 62282, locality PU 1149, López de Bertodano Formation, Seymour Island. (K) Right valve of bivalve *Solemya rossiana*, locality D5.345.2, López de Bertodano Formation, Seymour Island. All fossils whitened with ammonium chloride powder. Scale bars A-C = 10 mm; D-K = 20 mm.

Fig. 6. Images of petrographic thin sections from concretionary carbonate from sample DJ.633.3, Karlsen Cliffs Member, Snow Hill Island (A, C, D) and carbonate concretion D5.345.2 b1 from López de Bertodano Formation, Seymour Island (B). (A) Scanned image showing sedimentary matrix cemented by micritic cement cross-cut by putative fluid conduits infilled with multiple generations of banded and botryoidal fibrous calcite cement. (B) Scanned image of longitudinal cut through carbonate concretion showing micrite cemented sediment cross-cut by putative fluid conduit infilled with multiple generations of yellow coloured and translucent banded and botryoidal fibrous calcite cement. White box shows area of detail in Fig. 7D. (C,D) QEMSCAN® false colour mineralogical map based on the fieldscan analysis of thin section; mineralogical key to the colour codes used is indicated. (C) Map of the area of the thin section based on a 10 µm beam stepping interval. (D) More detailed 5 µm beam stepping interval fieldscan image of area indicated in (C) by white box. Scale bars: A-C = 10 mm.

Fig. 7. Photomicrographs of petrographic thin sections from concretionary carbonate from sample DJ.633.3, Karlsen Cliffs Member, Snow Hill Island (A-C) and carbonate concretion D5.345.2 b1 from the López de Bertodano Formation, Seymour Island (D). White arrows in all cases point towards the centres of fluid conduits. (A) Centre of fluid conduit infilling showing multiple generations of banded and botryoidal fibrous calcite cement (bbc) postdated by equant ferroan calcite (ec); plane polarised light image. (B) Centre of fluid conduit infilling showing banded and botryoidal fibrous calcite cement (bbc) postdated by probable ankerite cement (an) and then microcrystalline calcite cement (m2); plane polarised light image. (C) Fluid conduit showing wall of cemented sedimentary matrix (m1) cross-cut by banded and botryoidal fibrous calcite cement (bbc) with complex zonation revealed by luminescence, and later uniform orange luminescent equant ferroan calcite (ec); CL. (D) Edge of fluid conduit infilling showing sequential generations of yellow coloured banded and botryoidal fibrous calcite cement (ybbc) and translucent banded and botryoidal fibrous calcite cement (tbbc); plane polarised light image. The ybbc phase adjacent to the conduit wall (formed of cemented sedimentary matrix - m1) has recrystallized (rbbc), destroying the original fibrous crystal aggregations. Scale bars: A,B,D = 500 µm; C = 200 µm.

Fig. 8. Stable carbon and oxygen isotope cross plot from carbonate cemented sediments from Karlsen Cliffs Member, Snow Hill Island (SHI) and carbonate concretions from the López de Bertodano Formation, Seymour Island (SI).

Fig. 9. Gas chromatograms (total ion currents) of hydrocarbon fraction (A) and carboxylic acid fraction (B) from Thyasira Hill sample Sn1-1, Karlsen Cliffs Member, Snow Hill Island. Compound-specific $\delta^{13}C$ values are indicated in parentheses. (A) Circles: *n*-alkanes; black triangles: head-to-tail linked isoprenoids; white triangles: tail-to-tail linked isoprenoids; grey triangle: head-to-head-linked isoprenoid; PMI: pentamethylicosane; ; istd: internal standard. (B) Circles: *n*-fatty acids; white triangles: *iso*-fatty acids; black triangle: *anteiso*-fatty acid; white crosses: α,ω-diacids. C: contaminations; istd: internal standard; *i*: *iso*; *ai*: *anteiso.*

D 11: Tables

Table 0.1 Samples examined petrographically and geochemically.

Sample codes	Sample details	Location and reference	Stratigraphical unit	Analytical methods
DJ.616.22 DJ.616.34	'*Thyasira' townsendi* specimens	BAS section DJ.616, Thyasira Hill, Snow Hill Island; Lomas (1995)	Karlsen Cliffs Member, Snow Hill Island Formation	Petrography; C and O stable isotopes
Sn1-1, SHI-4, SHI-5, SHI-6, SHI-7	Concretionary sediment with '*Thyasira' townsendi* specimens	Thyasira Hill, Snow Hill Island; this paper	Karlsen Cliffs Member, Snow Hill Island Formation	C and O stable isotopes; organic biomarkers
DJ.731.14	Concretionary sediment	BAS locality DJ.731, Snow Hill Island; Pirrie et al. (1997)	Karlsen Cliffs Member, Snow Hill Island Formation	Petrography; C and O stable isotopes
DJ.633.3	Concretionary sediment	BAS locality DJ. 633.3, Snow Hill Island; Dingle (1995)	Karlsen Cliffs Member, Snow Hill Island Formation	Petrography; C and O stable isotopes
D5.345.2	Carbonate concretions	BAS locality DS. 345.2, Seymour Island;	López de Bertodano Formation	Petrography; C and O stable

		Bowman et al. (2012)		isotopes; XRD analysis
PRI 61054	Cements inside articulated '*Thyasira' townsendi* specimen	Zinsmeister collection, locality PU 1478, field no. 89-46	López de Bertodano Formation	Petrography; C and O stable isotopes
PRI 61078	Cements inside articulated *'Lucina' scotti* specimen	Zinsmeister collection, locality PU 1478, field no. 89-46	López de Bertodano Formation	C and O stable isotopes
PRI 60596	Cements inside articulated '*Thyasira' townsendi* specimen	Zinsmeister collection, locality PU1517, field no. 94-50	López de Bertodano Formation	C and O stable isotopes
PRI 58575	Cements inside articulated '*Thyasira' townsendi* specimen	Zinsmeister collection, locality PU K-104	López de Bertodano Formation, Unit KLB 7	C and O stable isotopes

Table 0.2 Stable isotope data for samples. Carbonate cement phases as used in text.

Sample code	Description	$\delta^{13}C$	$\delta^{18}O$
SHI-4B	Cemented sediment matrix (m1)	-18.4	-2.4

SHI-5B	Cemented sediment matrix (m1)	-16.2	-6.6
SHI-6B	Cemented sediment matrix (m1)	-16.2	-3.5
SHI-7A	Cemented sediment matrix (m1)	-14.8	-2.8
sn1-1b	Cemented sediment matrix (m1)	-15.0	-6.0
sn1-1b	Cemented sediment matrix (m1)	-15.6	-5.9
sn1-1a	Cemented sediment matrix (m1)	-15.6	-5.7
sn1-1a	Cemented sediment matrix (m1)	-15.5	-5.6
SHI-4A	'*Thyasira*' shell	-4.1	-5.5
SHI-5A	Later equant calcite cement (ec)	-12.2	-7.7
SHI-6A	Later equant calcite cement (ec)	-15.9	-5.6
SHI-6C	Later equant calcite cement (ec)	-2.9	-7.6
DJ.731.14	Fibrous calcite cement (bbc)	-15.7	-2.4
DJ.731.14	Fibrous calcite cement (bbc)	-17.2	-2.4
DJ.731.14	Later equant calcite cement (ec)	-10.7	-8.3
DJ.731.14	Fibrous calcite cement (bbc)	-15.7	-2.4
DJ.616.22	Fibrous calcite cement (bbc)	-20.4	-1.6
DJ.616.22	Fibrous calcite cement (bbc)	-11.7	-4.8

DJ.616.22	Later equant calcite cement (ec)	-6.8	-3.0
DJ.633.3	Fibrous calcite cement (bbc)	-14.4	-2.5
DJ.633.3	Fibrous calcite cement (bbc)	-16.4	-2.2
DJ.731.14	Fibrous calcite cement (bbc)	-11.9	-7.0
DJ.731.14	Later equant calcite cement (ec)	-10.8	-8.3
DJ.731.14	Later micro-sparry calcite cement (m2)	-13.5	-5.5
D5.345.2 a	Cemented sediment matrix (m1)	-46.7	0.3
D5.345.2 b1	Fibrous calcite cement (bbc)	-49.3	0.4
D5.345.2 b2	Cemented sediment matrix (m1)	-47.6	0.3
D5.345.2 b3	Fibrous calcite cement (bbc)	-36.1	-2.3
D5.345.2 b4	Fibrous calcite cement (bbc)	-47.0	-1.0
D5.345.2 c	Fibrous calcite cement (bbc)	-51.7	1.2
D5.345.2 d	Cemented sediment matrix (m1)	-47.0	0.2
D5.345.2 e1	Cemented sediment matrix (m1)	-42.4	0.1
D5.345.2 e2	Cemented sediment matrix (m1)	-42.3	0.5
D5.345.2 f	Cemented sediment matrix (m1)	-48.2	0.2
PRI 61054	Infilling fibrous calcite cement (bbc)	-58.0	2.2

PRI 58575	Infilling fibrous calcite cement (bbc)	-27.6	1.9
PRI 60596	Infilling fibrous calcite cement (bbc)	-24.6	0.9
PRI 61078	Infilling fibrous calcite cement (bbc)	-52.5	2.1

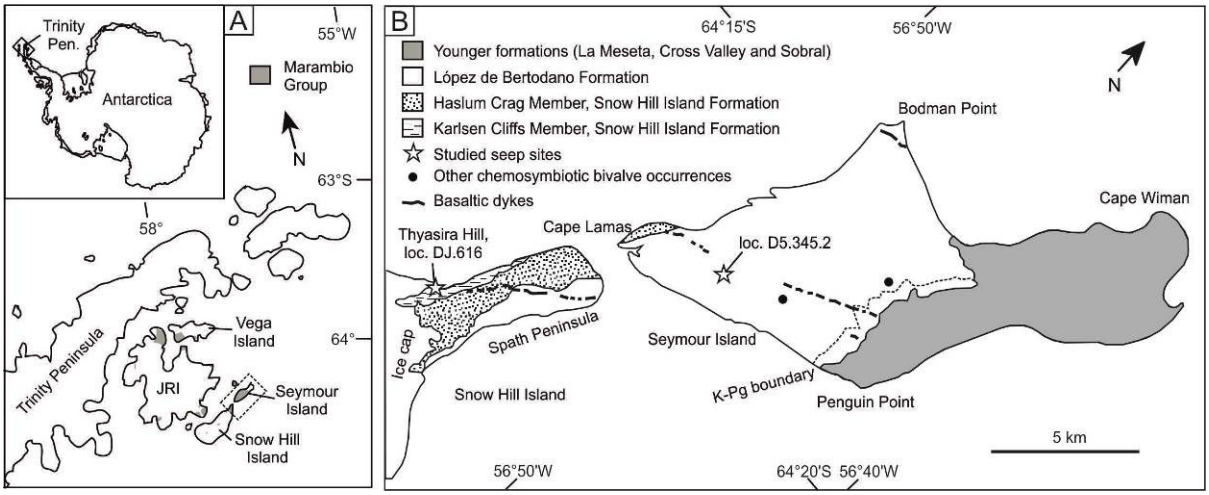
A
Trinity Pen.
Antarctica
55°W
Marambio Group
N
63°S
58°
64°
Vega Island
Trinity Peninsula
JRI
Seymour Island
Snow Hill Island
B
64°15'S
56°50'W
Younger formations (La Meseta, Cross Valley and Sobral)
López de Bertodano Formation
Haslum Crag Member, Snow Hill Island Formation
Karlsen Cliffs Member, Snow Hill Island Formation
Studied seep sites
Other chemosymbiotic bivalve occurrences
Basaltic dykes
N
Bodman Point
Cape Wiman
Thyasira Hill, loc. DJ.616
Cape Lamas
loc. D5.345.2
Ice cap
Spath Peninsula
Seymour Island
Snow Hill Island
K-Pg boundary
Penguin Point
5 km
56°50'W
64°20'S 56°40'W

Figure 0.1

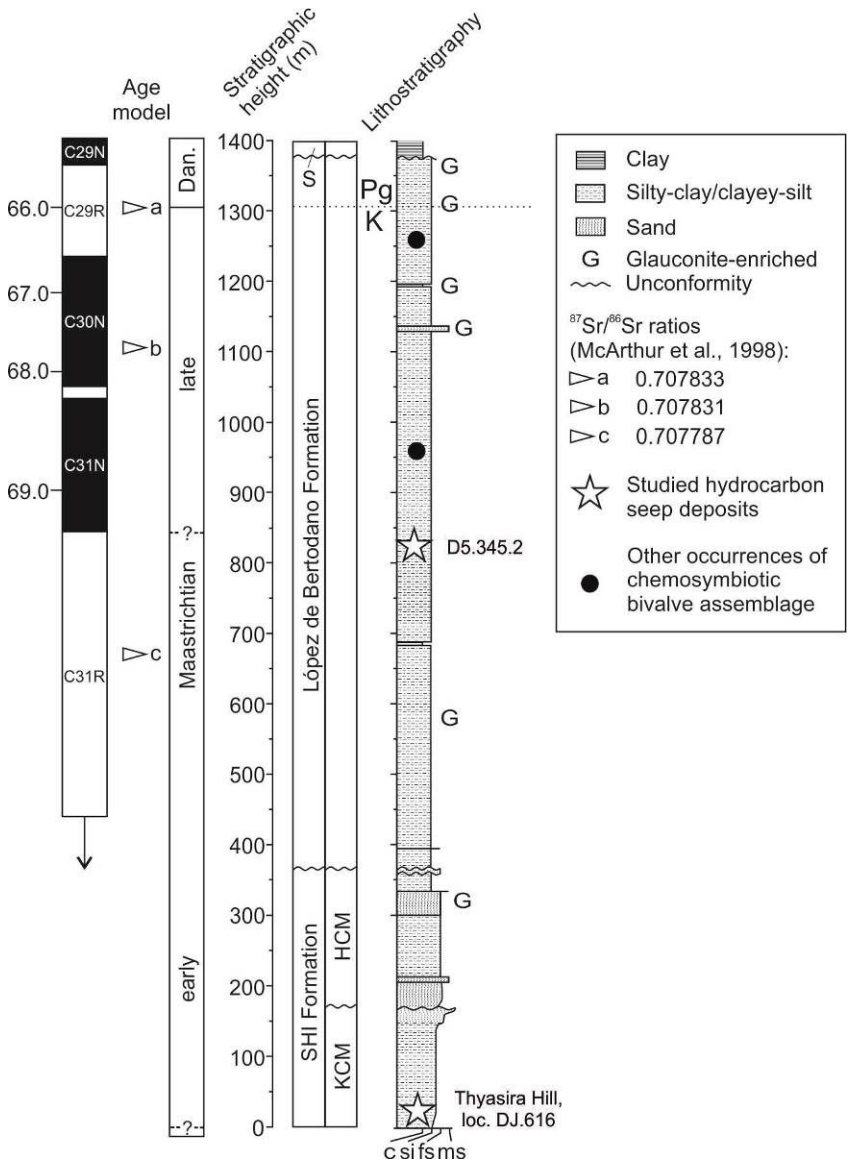
Age model
Stratigraphic height (m)
Lithostratigraphy
C29N
C29R
C30N
C31N
C31R
66.0
67.0
68.0
69.0
a
b
c
Dan.
late
Maastrichtian
early
?
?
1400
1300
1200
1100
1000
900
800
700
600
500
400
300
200
100
0
S
Pg
K
López de Bertodano Formation
SHI Formation
HCM
KCM
G
D5.345.2
Thyasira Hill, loc. DJ.616
c si fs ms
Clay
Silty-clay/clayey-silt
Sand
Glauconite-enriched
Unconformity
87Sr/86Sr ratios (McArthur et al., 1998):
a 0.707833
b 0.707831
c 0.707787
Studied hydrocarbon seep deposits
Other occurrences of chemosymbiotic bivalve assemblage

Figure 0.2

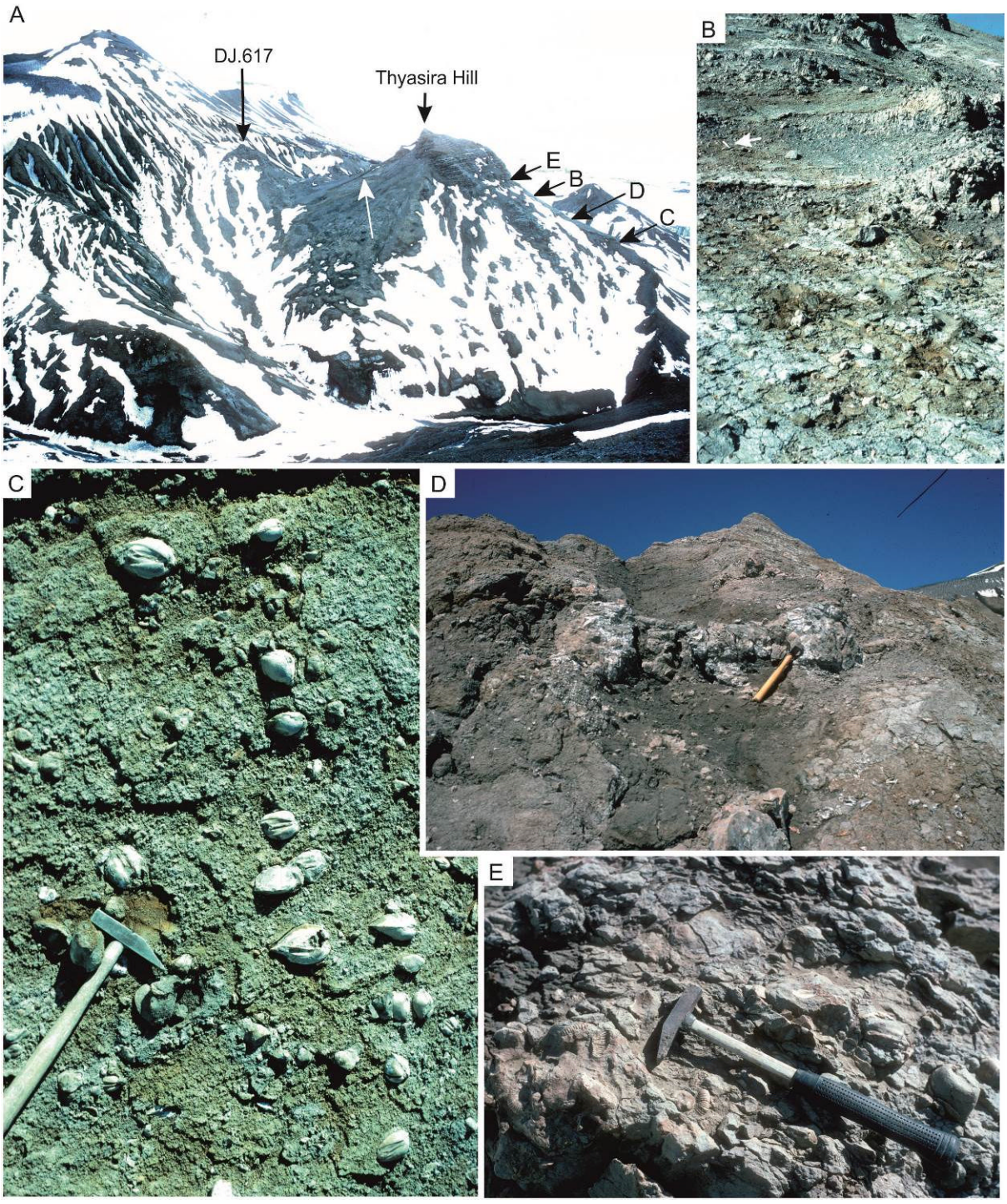

Figure 0.3

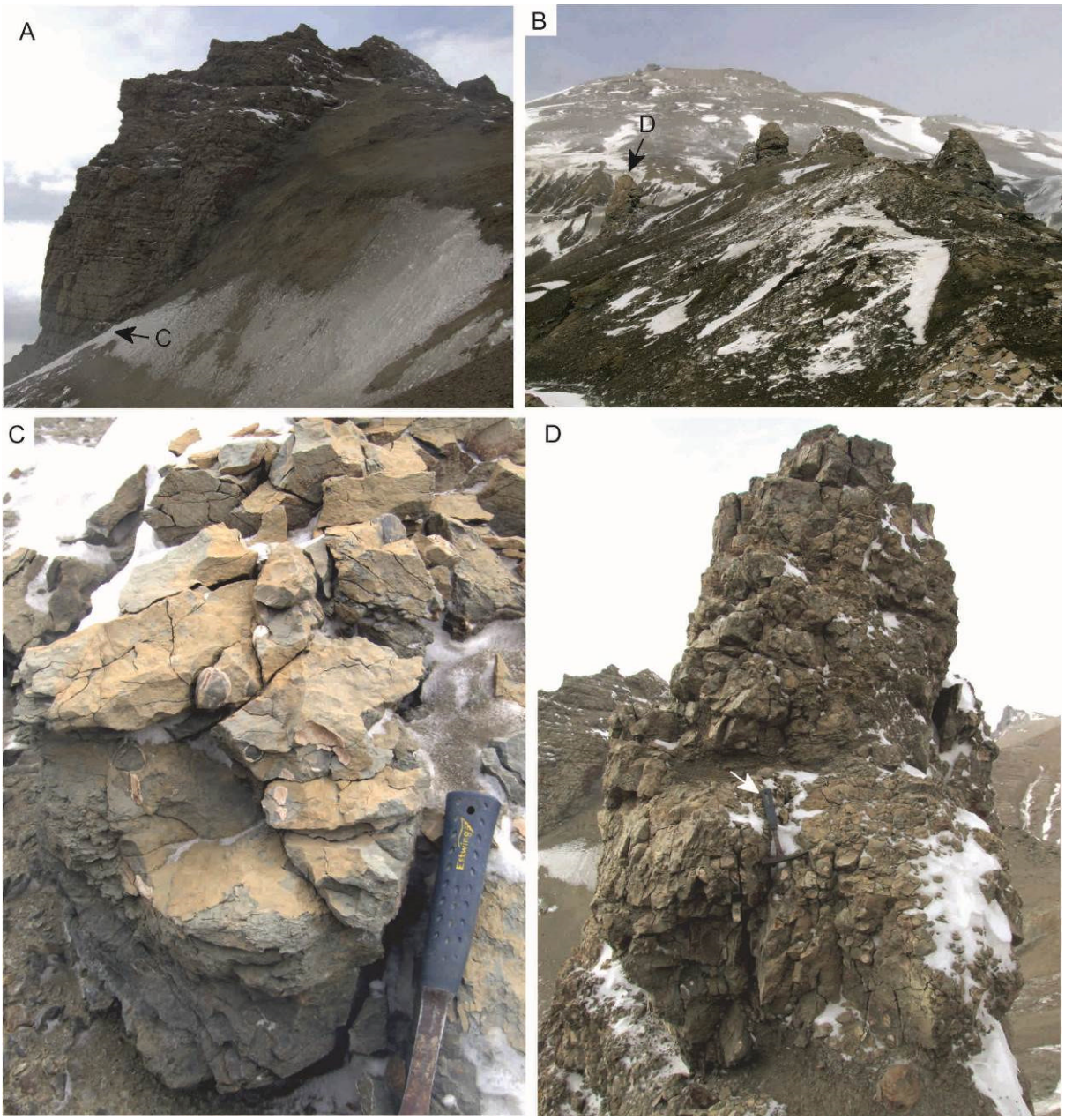

Figure 0.4

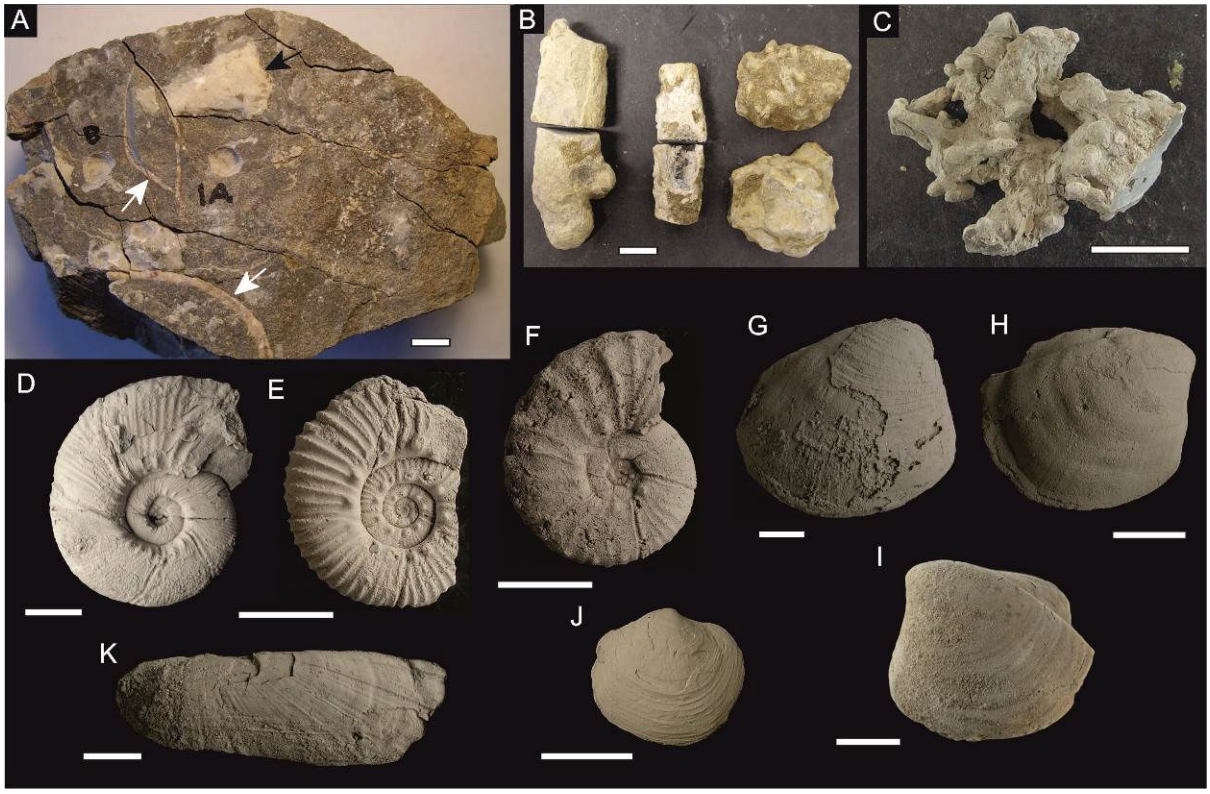

Figure 0.5

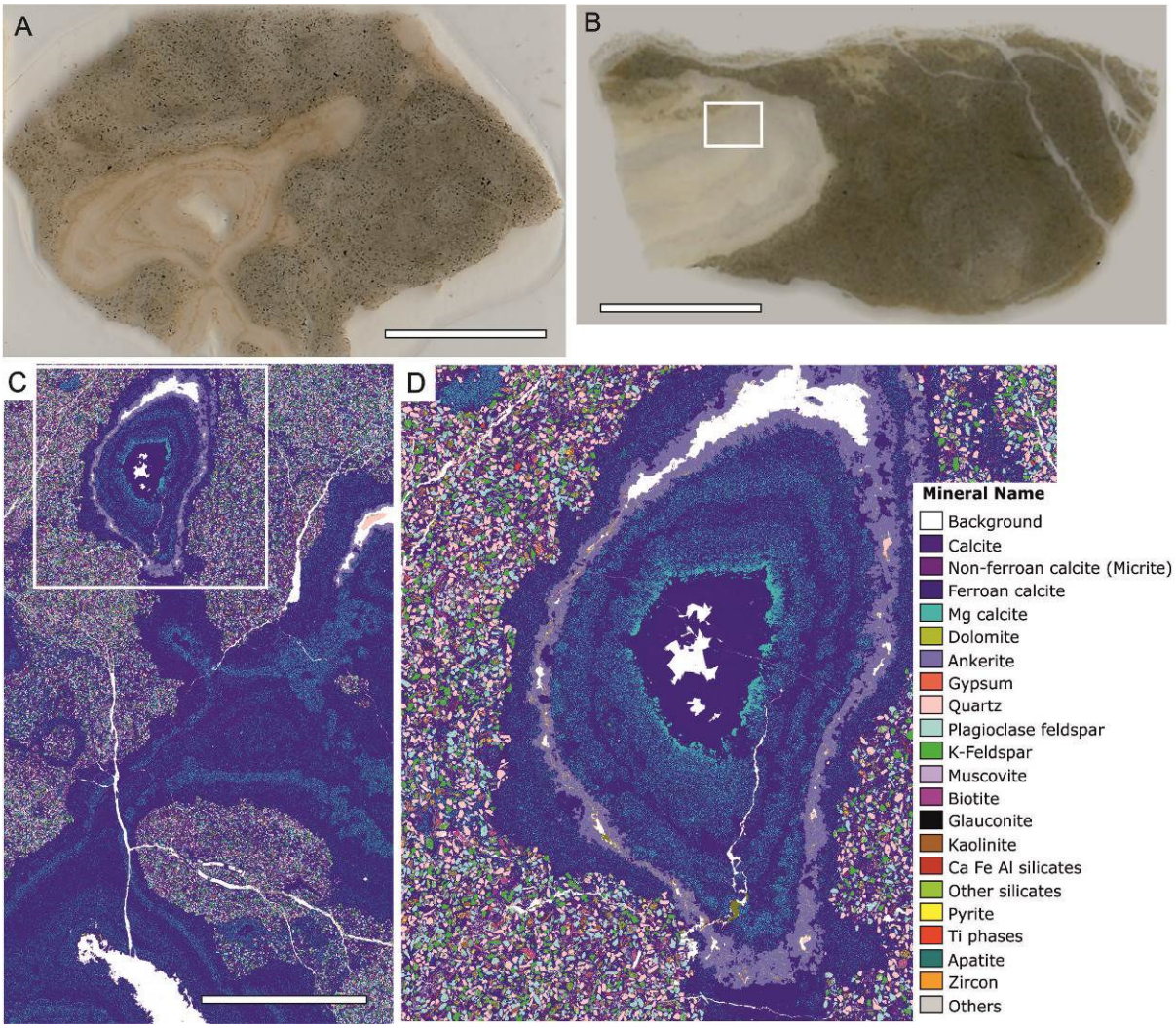
A
B
C
D
Mineral Name
Background
Calcite
Non-ferroan calcite (Micrite)
Ferroan calcite
Mg calcite
Dolomite
Ankerite
Gypsum
Quartz
Plagioclase feldspar
K-Feldspar
Muscovite
Biotite
Glauconite
Kaolinite
Ca Fe Al silicates
Other silicates
Pyrite
Ti phases
Apatite
Zircon
Others

Figure 0.6

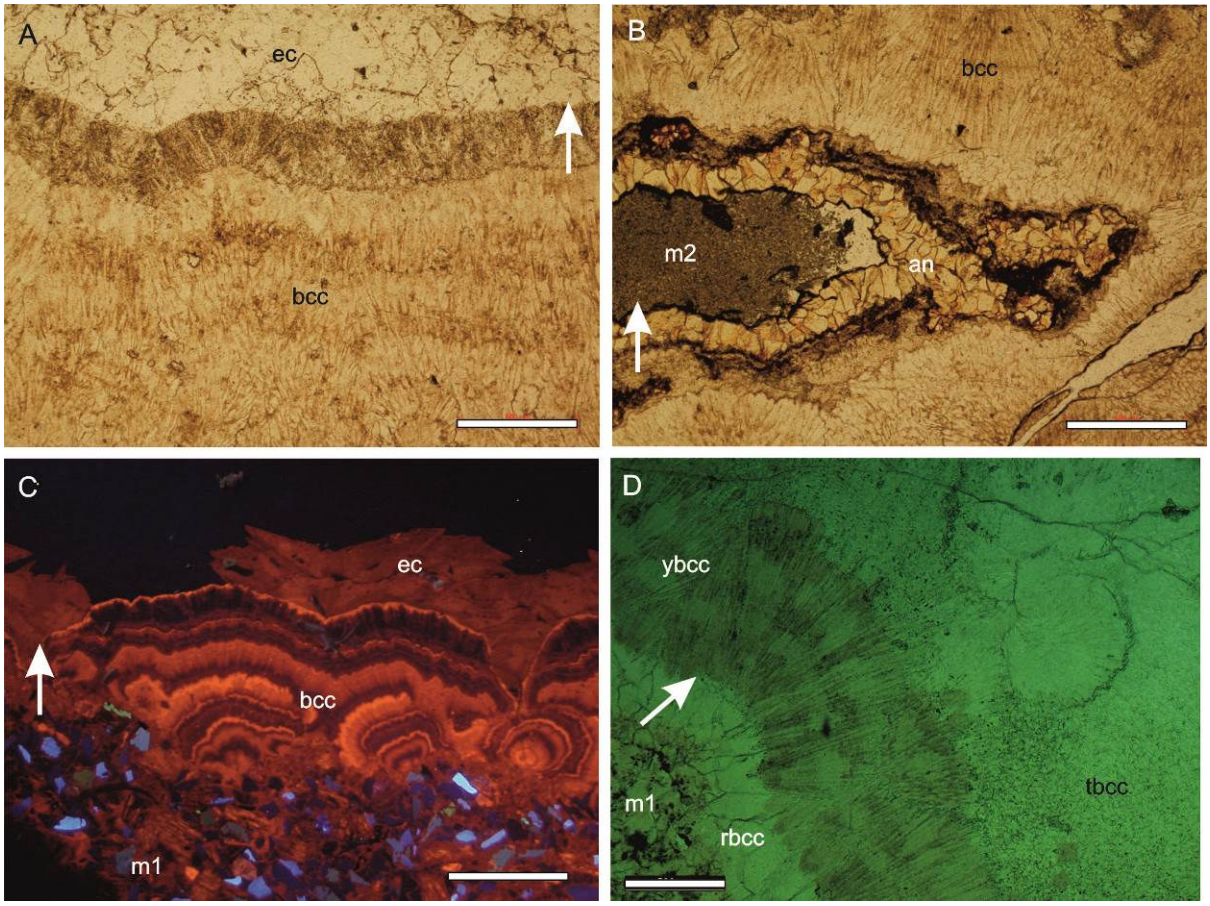

Figure 0.7

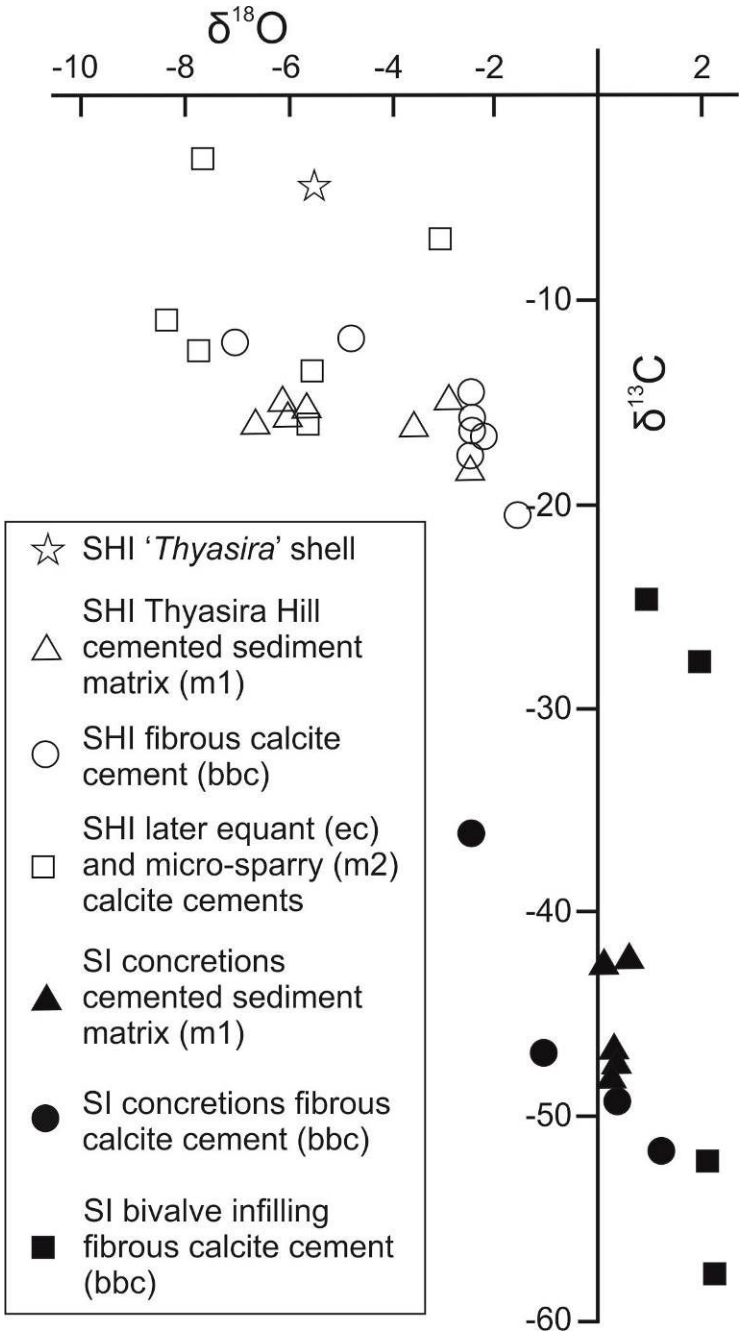
δ18O
-10
-8
-6
-4
-2
2
-10
-20
-30
-40
-50
-60
δ13C
SHI 'Thyasira' shell
SHI Thyasira Hill cemented sediment matrix (m1)
SHI fibrous calcite cement (bbc)
SHI later equant (ec) and micro-sparry (m2) calcite cements
SI concretions cemented sediment matrix (m1)
SI concretions fibrous calcite cement (bbc)
SI bivalve infilling fibrous calcite cement (bbc)

Figure 0.8

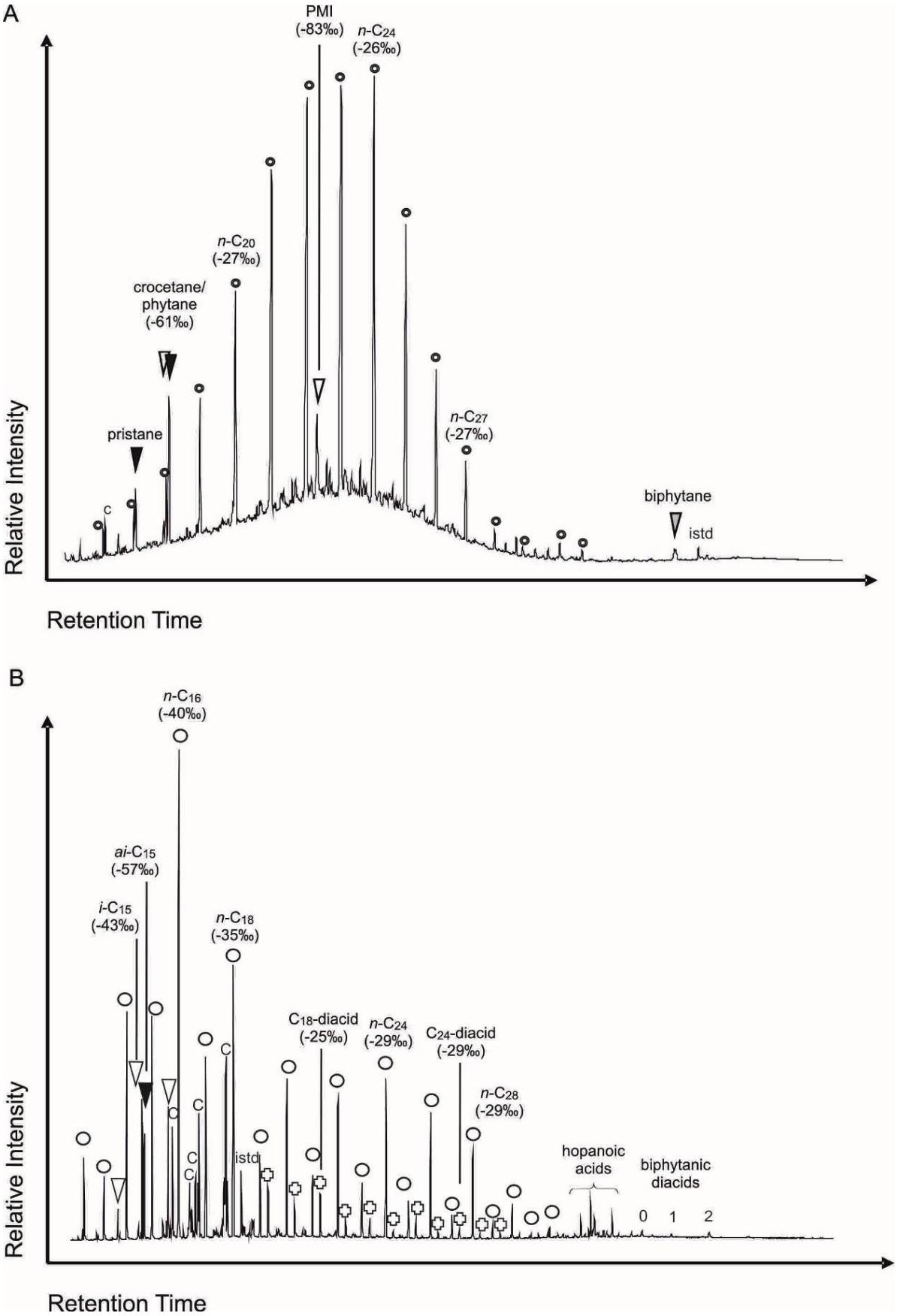
A
PMI
(-83‰)
n-C24
(-26‰)
n-C20
(-27‰)
crocetane/
phytane
(-61‰)
pristane
n-C27
(-27‰)
biphytane
istd
Relative Intensity
Retention Time
B
n-C16
(-40‰)
ai-C15
(-57‰)
i-C15
(-43‰)
n-C18
(-35‰)
C18-diacid
(-25‰)
n-C24
(-29‰)
C24-diacid
(-29‰)
n-C28
(-29‰)
istd
hopanoic
acids
biphytanic
diacids
0 1 2
Relative Intensity
Retention Time

Figure 0.9